UCL Université catholique de Louvain
Université partenaire de l'Académie universitaire 'Louvain'

Faculté de Pharmacie et des Sciences Biomédicales
Louvain Drug Research Institute
Pharmaceutics and Drug Delivery

HIGH-THROUGHPUT SCREENING OF EXCIPIENTS FOR THE FORMULATION OF PROTEIN-BASED VACCINES

Sébastien Dasnoy

Thèse présentée en vue de l'obtention du grade de
Docteur en Sciences Biomédicales et Pharmaceutiques

Promoteur : Véronique Préat
Co-promoteur : Dominique Lemoine

2012

TABLE OF CONTENTS

Pharm Res (2011) 28:1591–1605
DOI 10.1007/s11095-011-0393-x

RESEARCH PAPER

High-Throughput Screening of Excipients Intended to Prevent Antigen Aggregation at Air-Liquid Interface

Sébastien Dasnoy • Nancy Dezutter • Dominique Lemoine • Vivien Le Bras • Véronique Préat

Received: 26 October 2010 / Accepted: 3 February 2011 / Published online: 12 March 2011

ABSTRACT

Purpose The aim was to develop a high-throughput screening method compatible with low protein concentrations, as present in vaccines, in order to evaluate the performance of various excipients in preventing the aggregation at air-liquid interface of an experimental recombinant antigen called Antigen 18A.

Methods Aggregation of Antigen 18A was triggered by shaking in a half-filled vial or by air bubbling in a microplate. Size-exclusion chromatography, turbidimetry, Nile Red fluorescence spectroscopy, and attenuated total reflection Fourier-transform infrared spectroscopy were used to assess Antigen 18A aggregation. A high-throughput method, based on tryptophan fluorescence spectroscopy, was set up to screen excipients for their capability to prevent Antigen 18A aggregation at air-liquid interface.

Results While a similar aggregation profile was obtained with both stress tests when using size-exclusion chromatography, spectroscopic and turbidimetric methods showed an influence of the stress protocol on the nature of the aggregates. The high-throughput screening revealed that 7 out of 44 excipients significantly prevented Antigen 18A from aggregating. We confirmed the performance of hydroxypropyl-β-cyclodextrin and hydroxypropyl-γ-cyclodextrin, as well as poloxamers 188 and 407, in half-filled shaken vials.

Conclusions A high-throughput screening approach can be followed for evaluating the performance of excipients against aggregation of a protein antigen at air-liquid interface.

S. Dasnoy • V. Préat (✉)
Louvain Drug Research Institute, Université catholique de Louvain
Unité de Pharmacie Galénique, Avenue E. Mounier 73, UCL 7320
1200 Brussels, Belgium
e-mail: veronique.preat@uclouvain.be

N. Dezutter • D. Lemoine • V. Le Bras
GlaxoSmithKline Biologicals
Rue de l'Institut 89
1330 Rixensart, Belgium

KEY WORDS excipients · fluorescence spectroscopy · high-throughput screening · protein aggregation · vaccines

INTRODUCTION

From manufacturing to patient administration, vaccines may undergo various stress conditions that can impact antigen integrity and therefore vaccine efficacy (1). One major cause of protein instability is the formation of aggregates (2), which may result in a modified immunogenicity profile of the antigen (3). Ensuring antigen integrity is a critical factor that must be taken into account during the development of new vaccine candidates.

Proteins generally exhibit surface activity (4). In the presence of hydrophobic interfaces, they may be prone to denaturation by exposing their hydrophobic core, resulting in self-association and finally aggregation (2). Air-liquid interfaces can be present at different steps of the vaccine life, when mixing in vessels (manufacturing), dispensing in final containers (filling), during drying processes for solid formulations, during agitation for liquid formulations (shipping), and when freeze-dried formulations are reconstituted (handling).

Several proteins have been reported to aggregate at air-liquid interface, e.g. insulin (5–9), growth hormone variants (8,10–16), IgG variants (17–20), recombinant Factor VIII (21) and XIII (22), and IL-2 mutein (23). Various approaches have been used to study this phenomenon: shaking in the presence of headspace (6,7,16–24), vortexing (10,12,13) and nitrogen bubbling (11). Moreover, some excipients were shown to inhibit aggregation at air-liquid interface, such as polysorbate 20 (10,16,18,20), polysorbate 80 (16,17,19,21–23), poloxamer 407 (12), hydroxypropyl-β-cyclodextrin (10,15,19,24), hydroxypropyl-γ-cyclodextrin

(19), arginine (8), lysine (9), aspartic acid (7,9), glutamic acid (7,9), dextrose (6), and dextrates (6). This is only a limited list, and the use of high-throughput screening (HTS) technologies might provide opportunities for evaluating additional excipients.

With the same amount of antigen, an HTS approach offers the advantage to evaluate a larger number of conditions than with the classical analytical methods. HTS technologies have been used in developing stable formulations of monoclonal antibodies (25), therapeutic proteins (26), and vaccines (27). However, sensitivity issues may make some HTS analytical methods incompatible with the low antigen concentrations found in vaccines.

Antigen 18A is a 68-kDa recombinant glycoprotein consisting of 30% hydrophobic amino acid residues including 9 tryptophans. Its mean hydrophobicity index is 0.48 on the Kyte-Doolittle scale (28). Its experimental isoelectric point is 4.4±0.4, as determined by isoelectric focusing. Its melting temperature by differential scanning calorimetry is 56°C. After stability testing of 1 week at room temperature, neither adsorption of native Antigen 18A to the walls of glass vials nor aggregation was noticed.

Antigen 18A was shown to readily aggregate upon gentle shaking in a vial. The aim of this study was to evaluate the performance of various excipients in stabilizing this protein against aggregation at air-liquid interface. We first demonstrated by chromatographic, light scattering and spectroscopic techniques that conformational changes were involved in Antigen 18A aggregation at air-liquid interface. Then we proposed an HTS approach for testing excipients, based on tryptophan fluorescence spectroscopy. The selection of 44 excipients (amino acids, cyclodextrins, sugars, polyols, polymers and surfactants) was based on their presence in marketed parenteral drug products. Data management and analysis were automated to identify hit compounds from the screening. Further, Antigen 18A biological integrity was evaluated in the presence of these excipients in a shaken half-filled vial model.

MATERIALS AND METHODS

Materials

Antigen 18A was produced by GlaxoSmithKline Biologicals (Rixensart, Belgium). This protein was diluted from stock solution to 125 µg/ml in phosphate buffer (NaH_2PO_4/K_2HPO_4) 10 mM, pH 6.8, leading to a concentration equivalent to that in a common vaccine.

L-Arginine, L-aspartic acid, L-histidine, L-isoleucine, L-leucine, L-proline, L-serine, L-threonine and L-valine were purchased from Ajinomoto (Tokyo, Japan). L-alanine was obtained from Amresco (Solon, OH, United States) and L-glycine from Evonik Rexim (Ham, France). Polyethyleneglycol 15 hydroxystearate (*Solutol® HS15*), polyvinylpyrrolidones (PVP) K12 and K17 (*Kollidon®*), poloxamers (PX) 188 and 407 (*Lutrol®*) were gifts from BASF (Ludwigshafen, Germany). D-Mannitol was purchased from Roquette (Lestrem, France), D-sorbitol from Cargill (Minneapolis, MN, United States), sucrose from VWR (Leuven, Belgium), polysorbate (PS) 80 from NOF (Tokyo, Japan) and hydroxypropyl-γ-cyclodextrin (HP-γ-CD, *Cavasol® W8 HP*) from Wacker (Burghausen, Germany). Hydroxypropyl-β-cyclodextrin (HP-β-CD, *Kleptose® HPB*) was a gift from Roquette. Sulfobutylether-β-cyclodextrin (SBE-β-CD, *Captisol®*) was a gift from CyDex Pharmaceuticals, Inc. (Lenexa, KS, United States), polyoxyl 40 stearate (Myrj 52) was obtained from Croda (Goole, United Kingdom) and sodium dioctylsulfosuccinate (sodium docusate) was purchased from Cytec (Woodland Park, NJ, United States). Calcium chloride, magnesium chloride, magnesium sulphate, potassium hydrogenophosphate, ethanol, polysorbate 20, sodium caprylate, trehalose (Calbiochem), polyethylene glycols (PEG) 300, 600, 1,000, 1,500 and 6,000 were obtained from Merck (Darmstadt, Germany). Polyethylene glycols 400, 3,350 and 4,000 were gifts from Sasol (Johannesburg, South Africa). L-Glutamic acid, glycylglycine, L-lysine, *myo*-inositol, Nile Red (Fluka) and sodium dihydrogenophosphate were supplied by Sigma-Aldrich (Saint Louis, MO, United States). 3,3′,5,5′-Tetramethylbenzidine (TNB) was obtained from Biorad (Hercules, CA, United States). All solutions were prepared with water for injection obtained by triple distillation. Excipient solutions were filtered on a 0.22 µm polyether sulfone membrane (Sartolab, Sartorius Stedim, Aubagne, France). All excipients except glycylglycine were of compendial grade or tested following their respective Ph. Eur. monography prior to use. In the next sections, excipient concentrations presented in percentage were prepared on a weight-to-volume (w/v) basis.

Polypropylene (PP) deepwell microplates (Nunc) were obtained from ThermoFisher Scientific (Waltham, MA, United States), ultraviolet (UV)-transparent 96-well acrylic microtiter plates (Costar #3635) from Corning (Corning, NY, United States) and PP clear microplates (Whatman Uniplate) for pH measurement from GE Healthcare (Waukesha, WI, United States). PP troughs of 100 ml and PP disposable tips were purchased from Tecan (Männedorf, Switzerland). Type I glass vials were supplied by Nuova Ompi (Piombino Dese, Italy) and rubber stoppers from West Pharmaceutical Services (Lionville, PA, United States). UV-transparent seals (VIEWseal) were purchased from Greiner Bio-one (Kremsmünster, Austria). Teflon-stoppered 10×2 mm quartz cells were obtained from Hellma (Müllheim, Germany).

Size-Exclusion Chromatography

Size-exclusion high performance liquid chromatography (SEC) measurements were performed on an Agilent 1,200 chain (Santa Clara, CA, United States). A TSKgel PWXL guard column (6 mm ID × 4 cm) was placed in front of a TSKgel G3000PWXL column (7.8 mm ID × 30.0 cm) from TOSOH (Tokyo, Japan) and loaded with a volume of 100 µl. Phosphate-buffered saline (PBS), pH 7.4, was used as mobile phase at a flow rate of 0.5 ml/min. The elution profile was monitored at 213 nm by a diode array detector. Data acquisition and peak integration calculations were performed using the Chemstation (Agilent) software. In preliminary experiments with multi-angle light scattering and refractive index detectors connected in series, the molecular weight of eluted species was determined (data not shown). The main peak of native protein (elution time 13.4 min) was assigned to monomeric species. Higher molecular weight species eluted at 11.5 min were defined as soluble aggregates. The percentage of those two populations was calculated by reporting the integrated peak area values to the total area under the curve recovered for the non-shaken sample. The extinction coefficients of the monomer and soluble aggregates were considered identical. Protein mass recovery was calculated by dividing the sum of monomer and soluble aggregate peak areas by the total area under the curve of the non-shaken sample.

Turbidimetry

Optical density measurements were performed in a quartz cell on a UV-visible spectrophotometer Ultrospec 2100pro (GE Healthcare). Spectra were recorded at room temperature between 200 and 400 nm, at a speed of 1,500 nm/min and with a scanning step of 0.5 nm. The matrix signal (placebo, antigen-free solution) was subtracted. Sample turbidity was assessed at 350 nm (OD_{350}), as the signal at this wavelength is not due to chromophoric absorption but to light scattering.

Right-angle light scattering (RALS) measurements were performed in a quartz cell, on a LS50b spectrofluorometer (Perkin Elmer, Waltham, MA, United States) equipped with a four-cell holder thermostated at 25°C by a water-circulating bath (Julabo, Seelbach, Germany). A scan synchronized in wavelength was performed between 450 and 650 nm. In this configuration, the signal reaching the detector located at 90° only originates from light scattering (29). The excitation and emission slits were both set at 2.5 nm, the scanning step at 0.5 nm and the scanning speed at 1,500 nm/min. Each spectrum was the average of five consecutive scans. The matrix signal was subtracted. A wavelength of 500 nm was selected as a good compromise between sensitivity and signal stability.

Absorption Spectroscopy

Analyses were performed at 25°C on a Varioskan Flash microplate reader (ThermoFisher Scientific, Waltham, MA, United States). The bandwidth and integration time were set at 5 nm and 100 ms, respectively. The matrix signal was subtracted.

Sample pathlength (L) was obtained by measuring the water absorption peak in the near-infrared region at 975 nm, corrected for baseline at 900 nm (30). The obtained value was not classically expressed in length units but as a height of water peak in absorbance units (AU). A dose range experiment with Antigen 18A allowed us to calculate an apparent extinction coefficient at 280 nm (ε) of 7.5 10^{-3} $AU^{-1}.\mu g^{-1}.ml$ in phosphate buffer. The protein chromophoric absorbance at 280 nm (A_{280}) was calculated by measuring the optical density at 280 nm corrected for light scattering at 320 nm. Based on the Lambert-Beer law, sample concentration (C) can be calculated with Eq. 1.

$$C = \frac{A_{280}}{\varepsilon L} = \frac{1}{\varepsilon}\left(\frac{A_{280}}{A_{975}}\right) = \frac{1}{\varepsilon}\left(\frac{OD_{280} - OD_{320}}{OD_{975} - OD_{900}}\right) \quad (1)$$

Compared with classical absorbance measurements in spectroscopic cells, sample composition may influence the meniscus shape and therefore the pathlength and apparent extinction coefficient. For this reason, this technique was only used for following variations in protein concentration on a well-to-well basis.

Tryptophan Fluorescence Spectroscopy

Measurements were performed at 25°C in a Varioskan Flash microplate reader (ThermoFisher Scientific). While a higher signal-to-noise ratio was obtained by exciting Antigen 18A at its wavelength of maximum absorption (282 nm), a selective excitation of tryptophan residues at 295 nm (29) showed a higher repeatability in preliminary studies (data not shown). The excitation and emission wavelengths were 295 nm and 336 nm, respectively. The excitation slit was set at 12 nm and the integration time at 500 ms. Bottom optics were used to be independent of sample volume variations.

Nile Red Fluorescence Spectroscopy

Nile Red emission and anisotropy were measured. Preliminary studies showed that no inner filter effect was observed at the dye concentration used in both techniques. Emission measurements were performed in microplate at 25°C in a Varioskan Flash microplate reader (ThermoFisher Scientific) equipped with an automated dispenser. The sample initial volume was 150 µL, to which 2 µL of Nile Red from a 100 µM ethanolic solution were added with the primed

dispenser, leading to a final concentration of 1.3 µM Nile Red in solution. The plate was shaken at 300 rpm during 30 s and left at room temperature for 5 min prior to starting analysis. The excitation wavelength was set at 575 nm and the excitation slit at 12 nm. Emission scans were recorded between 600 and 700 nm, with a scanning step of 1 nm and an integration time of 500 ms. The top optics were used. In preliminary trials, we verified that neither the presence of Nile Red nor the sample preparation impacted the protein conformation (tryptophan fluorescence) and aggregation state (optical density). Raw scan values were exported for subsequent spectral processing and analysis with customized macros developed in Visual Basic (Microsoft, Redmond, WA, United States). Both the matrix signal in the presence of Nile Red and the light scattering contribution from dye-free samples were subtracted. Difference spectra were obtained by subtracting the spectrum of the non-stressed sample from the spectra of stressed samples and revealed that main changes in intensity occurred at 625 nm. This wavelength was selected for studying variations in fluorescence intensity. Spectra were first smoothed with a seven-points filter and third degree Savitky-Golay polynomial and then the intensity at 625 nm extracted. The centre of gravity of the emission ($\langle\lambda\rangle$) was calculated by the centre of spectral mass position ($\overline{\nu}_{csm}$) method (Eq. 2). Bandpass correction was applied when converting intensities (I) from wavenumbers ($\overline{\nu}$) to wavelength (λ) units (29). No smoothing was required, as the noise regular pattern has a low impact on the centre of spectral mass position. Compared with the emission wavelength of maximum intensity, this approach does not involve any mathematical transformation of raw data and allows a better detection of subtle changes in the spectral shape.

$$\langle\lambda\rangle = \frac{1}{\overline{\nu}_{csm}} = \frac{\sum I(\overline{\nu})}{\sum \overline{\nu} I(\overline{\nu})} = \frac{\sum \lambda^2 I(\lambda)}{\sum \lambda I(\lambda)} \quad (2)$$

Anisotropy measurements were performed in a quartz cell, on a LS50b spectrofluorometer (Perkin Elmer) equipped with a four-cell holder thermostated at 25°C by a water-circulating bath (Julabo). Just prior to analysis, 5 µL Nile Red from a 100 µM ethanolic solution were added to 495 µL sample, leading to a final dye concentration of 1 µM. The cell content was homogenized by gentle mixing. The excitation wavelength was set at 575 nm, the slits at 15 nm (excitation) and 20 nm (emission), the scanning step at 0.5 nm and the scanning speed at 300 nm/min. For each sample, four different spectra were recorded from 600 to 625 nm with the following excitation/emission polarizer combinations: I_{hh}, I_{vv}, I_{hv} and I_{vh}. Indices are related to horizontal (h) and vertical (v) positions. Each spectrum was the average of five consecutive scans. Anisotropy spectra were obtained by calculating anisotropy (r) at each wavelength (Eq. 3) (29):

$$r = \frac{I_{vv} - GI_{vh}}{I_{vv} + 2GI_{vh}}, \text{ with } G = \frac{I_{hv}}{I_{hh}} \quad (3)$$

Difference spectra revealed that the main changes in anisotropy occurred at 605 nm. This wavelength was selected for studying variations in fluorescence anisotropy. In preliminary studies, we observed that the present scanning approach allowed us to get more repeatable results than a direct measurement of anisotropy at 605 nm.

ATR-FTIR Spectroscopy

Samples were analyzed on a Tensor 27 Fourier-transform infrared (FTIR) spectrometer equipped with an attenuated total reflection (ATR) module (Bruker, Ettlingen, Germany). The detector was cooled with liquid nitrogen and the chamber purged with dry air. Each spectrum was the average of 256 scans recorded from 4,000 to 400 cm^{-1}. A sample volume of 3 µL was poured onto the ZnSe crystal, and water was evaporated by flushing with dry nitrogen. The effect of adsorption to ZnSe crystal on Antigen 18A conformation was not evaluated. Each sample was analyzed in triplicate. A baseline was recorded before each triplicate measurement. Based on a Student's statistical test (α=0.01), the Kinetics application (31) was used to highlight significant differences in the Amide I (1,710–1,600 cm^{-1}) region that is known to be sensitive to protein secondary structure (carbonyle stretching). The OPUS software (Bruker) was used for data acquisition, subtraction of matrix signal, averaging of triplicate spectra and offset correction. Spectra were exported for subsequent processing with customized macros developed in Visual Basic (Microsoft). After a linear baseline correction, the second-derivative spectra were calculated with a nine-points filter and second degree Savitky-Golay polynomial, smoothed with the same polynomial and then vector-normalized in the Amide I region. The similarity between second-derivative spectra was studied by the area of overlap method (32).

Enzyme-Linked Immunosorbent Assay

A direct sandwich enzyme-linked immunosorbent assay (ELISA) method was applied to evaluate the integrity of Antigen 18A epitopes. Antigen 18A samples were incubated overnight in the presence of an excess of primary polyclonal antibody (commercial source). The samples were transferred in microplates (MaxiSorp, Nunc, ThermoFisher Scientific) coated with a defined quantity of Antigen 18A before the secondary antibody coupled with peroxidase

(Sigma-Aldrich) was added. After addition of the peroxidase substrate (TMB), the intensity of the colorimetric reaction was measured in a spectrophotometer (Versamax, Molecular Devices, Sunnyvale, CA, United States) at 450 and 620 nm. The calibration curve was fitted to a sigmoid by the four-parameter method in the SoftMax Pro software (Molecular Devices), and allowed the calculation of the concentration of native Antigen 18A.

High-Throughput Screening

A series of 44 excipients were evaluated at six different concentrations in triplicate. For each condition, a single placebo was prepared and used as a blank to be subtracted in spectroscopic analyses. In preliminary studies, variability in edge wells was 2% higher than in inner wells. The outer rows were reserved for blanks. On each plate, one well by row was dedicated to the excipient-free control sample (inner rows, six wells) or its associated blank (outer rows, two wells).

The screening was performed on a total of 12 plates. A customized application developed in Visual Basic (Microsoft) randomized all conditions and generated XML worklists containing liquid volumes to be added in each well. Replicates were located on different plates.

All samples contained phosphate buffer (NaH_2PO_4/K_2HPO_4) 10 mM, pH 6.8. The stock solution concentrations were the following: 100 mM phosphate buffer, 0.5% surfactants, 3% polymers, 15% polyols except 12% inositol, 15% carbohydrates and cyclodextrins, 10 mM calcium and magnesium salts, 250 mM sodium chloride, 3 mM aspartic acid, 50 mM glutamic acid, 150 mM leucine, 250 mM isoleucine and 500 mM other amino acids.

Based on the XML worklists processed by a Visual Basic application (Microsoft) and subsequently imported into the Gemini software (Tecan), a Genesis liquid handling station equipped with an eight-tip liquid handling (LiHa) arm (Tecan) prepared excipient mixes at a volume of 1,000 µL in deepwell microplates.

The transfer from deepwell to microtiter plates was performed with a 96-channel head (TeMo) equipped with disposable tips (Tecan). From a deepwell stock plate, the antigen or equivalent buffer volume was added to the microtiter plates with the TeMo. Two microtiter plates were prepared from a deepwell microplate, one for air-bubbling stress test and the other for pH check. The air-bubbling and pH plates were filled with 150 µL/well and 200 µL/well, respectively. In the latter, pH measurement was automatically performed in each well with a probe adapted to a MiniPrep station (Tecan).

The air-bubbling plates were analyzed by ultraviolet spectroscopy and tryptophan fluorescence spectroscopy before and after stress test. A custom application developed in Visual Basic (Microsoft) allowed processing and analysis of data generated from the HTS study, as such identifying hit conditions with a statistical approach.

Air-Liquid Interface Stress Test

The behaviour of Antigen 18A at the air-liquid interface was studied in vials closed with rubber stoppers and sealed with aluminium crimps. The vials were filled at half (1.5 ml) or at maximum (3.625 ml as determined by weighing) volume. Then they were tape-fixed horizontally on an agitating plate and shaken at 200 rpm. During kinetics studies, vials were picked up randomly every 15 min for analysis.

In microplate, air bubbling was performed with the TeMo head. A series of air bubbles (30 µL) was blown in each well, with a periodicity of 1 min. After this stress test, microplates were sealed and centrifuged during 5 min at 1,000 rpm for eliminating residual air bubbles. Preliminary tests showed that centrifugation did not impact the spectroscopic measurements.

Statistical Analysis

Parametric tests are based on sample independence, normality and homoscedasticity assumptions. Raw data were first analyzed by the Box-Cox method in Design Expert (Stat-ease, Minneapolis, MN, United States) in order to test if power or logarithmic transformations are able to improve the normality profile of the residuals frequency distribution. In case a transformation was identified, it was applied to the data. All subsequent calculations were performed with the Unistat Excel add-in (Unistat, London, United Kingdom). The normality hypothesis was verified by the Shapiro-Wilk test. Moderate non-normality was accepted in case the skewness [−1.5;1.5] and kurtosis [−1;2] values were not too far from the null value (33). The homogeneity of variance hypothesis was evaluated by the Cochran test. After verification of normality and homoscedasticity conditions, an analysis of variance (ANOVA) followed by a Dunnett test approach was adopted. All statistical tests were performed with a risk factor $\alpha = 5\%$. In the HTS study, the ANOVA-Dunnett approach ($\alpha = 1\%$) was adapted to automation in Visual Basic (Microsoft).

The HTS study encompassed 72 excipient-free controls (six by plate) that allowed us to determine the repeatability (intraplate), reproducibility (interplate) and global variability (intraplate + interplate) of the screening. These parameters were calculated based on an ANOVA approach.

The z'-value is a common adimensional parameter used for evaluating the quality of an HTS assay. Based on the mean (μ) difference and variability (σ) of positive ($C+$) and

negative (*C–*) controls, a separation band was calculated, based on Eq. 4. The identification of hits by an HTS method is considered as feasible when z'-values are greater than or equal to 0.5 (34).

$$z' = 1 - 3\frac{(\sigma_{C+} + \sigma_{C-})}{|\mu_{C+} - \mu_{C-}|} \quad (4)$$

RESULTS

Aggregation Kinetics in a Shaken Vial

The influence of an air-liquid interface on Antigen 18A aggregation kinetics was studied by filling vials with different volumes of protein solution. Vials were tape-fixed horizontally on an agitating plate and shaken during 5 h 45 min, in the presence (half volume) or absence (maximum volume) of air-liquid interface. The non-shaken sample was used as a reference for statistical analyses.

The protein aggregation kinetics during shaking were followed by SEC (Fig. 1). In half-filled vials only, the monomer gradually degraded while soluble aggregates formed. Significant differences with the control were detected in both populations from 1 h of shaking ($p<0.05$). A significant loss in protein mass recovery was observed from 3 h 30 min of shaking ($p<0.05$).

Whatever the filling volume in vials, no change in turbidity was detected by visual inspection during the whole experiment. However, in half-filled vials, an increase in turbidity with shaking time was observed from 2 h 15 min by right-angle light scattering and from 3 h 30 min by optical density ($p<0.05$) (Fig. 2).

The influence of shaking on Antigen 18A tertiary structure was followed by tryptophan fluorescence spectroscopy. No significant change ($p>0.05$) in tryptophan emission was observed (data not shown).

Shaking-induced conformational changes of Antigen 18A were observed in half-filled vials by Nile Red fluorescence spectroscopy (Fig. 3). For thermodynamic reasons, hydrophobic regions generally are barely exposed to water when proteins are in their native conformation. When a protein denatures or unfolds, hydrophobic patches may become more exposed to the solvent. Changes in protein surface hydrophobicity, associated with protein denaturation and aggregation can be detected by an increased affinity for Nile Red, a non-ionic hydrophobic fluorescent dye (35,36). Recently, this technique was used in high-throughput protein formulation screening (26). Upon shaking in half-filled vials, we observed ($p<0.05$) an increase in Nile Red fluorescence intensity from 1 h 30 (Fig. 3b), a blue-shift in the center of gravity of emission from 30 min (Fig. 3c), and an increase in anisotropy from 1 h (Fig. 3d). Those parameters reflect a change in the environment of the dye molecules: increase in hydrophobicity (intensity) and polarity (blue-shift), as well as decrease in mobility (anisotropy) (29).

The protein secondary structure of Antigen 18A was also modified by shaking vials in the presence of air-liquid interface, as evidenced by changes in the Amide I region of ATR-FTIR spectra (Fig. 4a). The relative contribution of absorbing species was studied, based on vector-normalized second-derivative spectra (Fig. 4c). The native structure was characterized by a main peak at 1,637 cm^{-1} that we assigned to the presence of β-sheet. Three other minor peaks were attributed to β-sheet or turns (1,668 cm^{-1} and 1,686 cm^{-1}), and α-helix or random coil structures

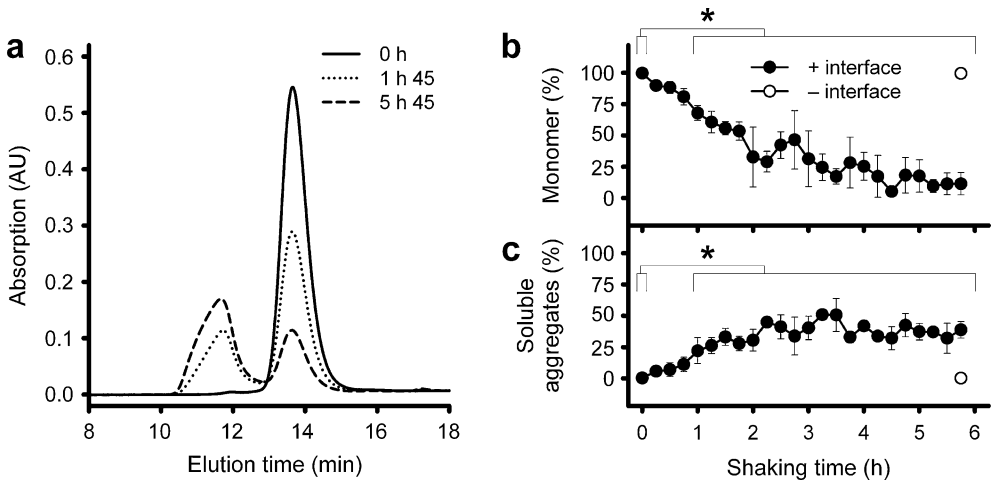

Fig. 1 Influence of air-liquid interface on Antigen 18A aggregation profile by size-exclusion chromatography, in a shaken vial model. (**a**) Chromatograms (UV signal at 213 nm) obtained from a half-filled vial before (0 h) and after shaking (1 h 45 min and 5 h 45 min). The matrix signal was subtracted. Evolution of monomer (**b**, elution time: 13.4 min) and soluble aggregates (**c**, elution time: 11.5 min) during shaking of vials filled at half and maximum volume. *Error bars* represent the standard deviation from three independent experiments. In the presence of interface, the *star symbol* indicates significant difference with the non-shaken control ($p<0.05$) by ANOVA-Dunnett analysis.

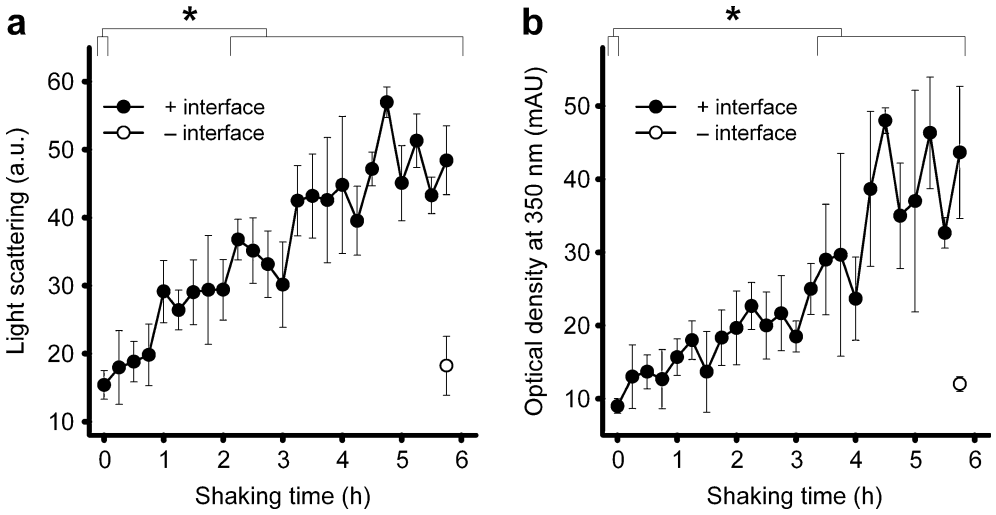

Fig. 2 Influence of air-liquid interface on Antigen 18A aggregation by right-angle light scattering at 500 nm (**a**) and optical density at 350 nm (**b**), in a shaken vial model. *Error bars* represent the standard deviation from three independent experiments. In the presence of interface, the *star symbol* indicates significant difference with the non-shaken control ($p < 0.05$) by ANOVA-Dunnett analysis.

(1,652 cm^{-1}) (37,38). The minor peak detected at 1,700 cm^{-1} was not attributed. During shaking, all these peaks gradually disappeared, and a large peak ($p<0.01$) concomitantly appeared at 1,632 cm^{-1}, which was assigned to β-sheet. In zero-order spectra, reorganization in the β-sheet region was reflected by the 1,632/1,637 cm^{-1} ratio that increased from 1 h 15 ($p<0.05$) (Fig. 4b). A loss in spectral similarity was noticed (Fig. 4d). Taken as a whole,

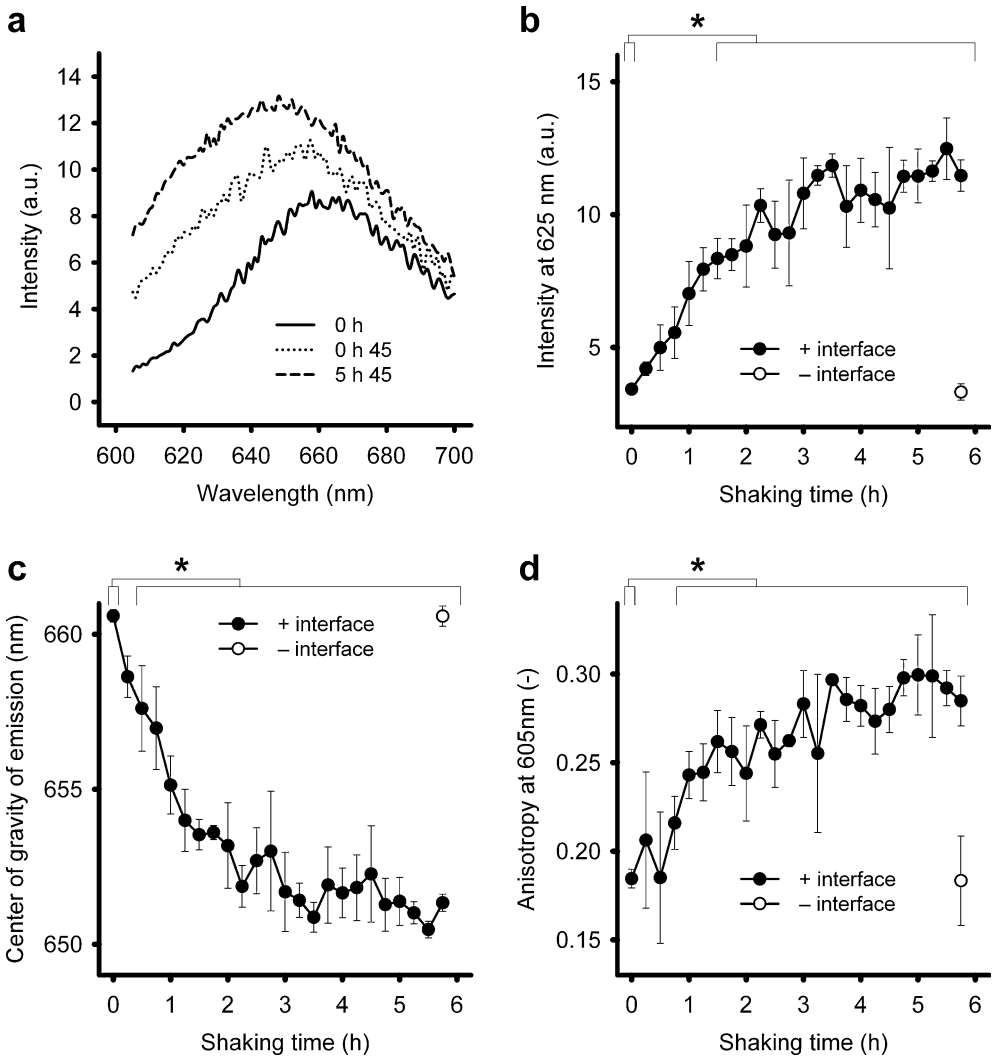

Fig. 3 Influence of air-liquid interface on Antigen 18A surface hydrophobicity by Nile Red fluorescence spectroscopy, in a shaken vial model. Emission scans (**a**) obtained from a half-filled vial before (0 h) and after shaking (0 h 45 min and 5 h 45 min), from which intensity at 625 nm (**b**) and the centre of gravity of emission (**c**) are extracted. Evolution of anisotropy at 605 nm (**d**) upon shaking. *Error bars* represent the standard deviation from three independent experiments. In the presence of interface, the *star symbol* indicates significant difference with the non-shaken control ($p < 0.05$) by ANOVA-Dunnett analysis.

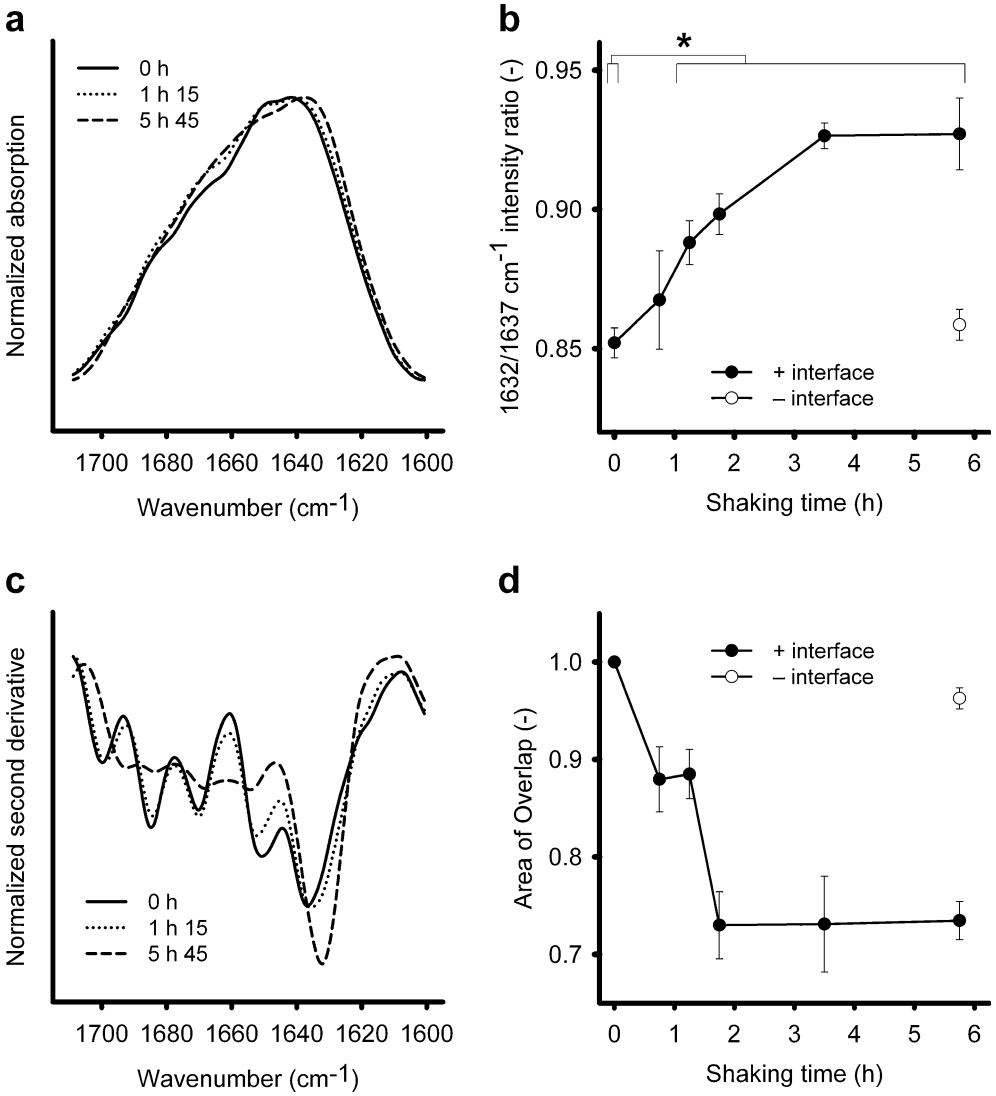

Fig. 4 Influence of air-liquid interface on Antigen 18A secondary structure by attenuated total reflection Fourier-transform infrared spectroscopy, in a shaken vial model. Normalized absorption spectra (**a**) obtained from a half-filled vial before (0 h) and after shaking (1 h 15 min and 5 h 45 min) from which the 1,632/1,637 cm^{-1} intensity ratio is extracted (**b**). Vector-normalized second-derivative spectra (**c**) from which the area of overlap is calculated (**d**). *Error bars* represent the standard deviation from three independent experiments. In the presence of interface, the *star symbol* indicates significant difference with the non-shaken control ($p < 0.05$) by ANOVA-Dunnett analysis. The intrinsic normalization of area of overlap precluded a statistical comparison to the non-shaken sample.

we observed an increase of the relative contribution of β-sheet structures with shaking time in half-filled vial.

In conclusion, Antigen 18A structural stability was studied upon shaking in the presence or absence of air-liquid interface. After 5 h 45 min of shaking, changes in Antigen 18A aggregation profile, tertiary and secondary structure ($p<0.05$) due to the air-liquid interface were emphasized with a combination of chromatographic, light scattering and spectroscopic techniques.

Aggregation Kinetics in a Microtiter Plate

In order to protect Antigen 18A against aggregation at air-liquid interface, we aimed at developing an HTS approach for rapidly evaluating the performance of a large number of excipients.

The first step was to develop a stress test in microplate to follow protein aggregation at air-liquid interface. After unsuccessful trials to aggregate Antigen 18A by plate shaking or vortexing, air-liquid interface was created in wells by air bubbling. Basically, air was first aspirated in tips mounted on a 96-channel head and then blown synchronously in all the wells of a microplate. As polysorbate 80 solutions rapidly foam up upon air bubbling, we used this surfactant for optimizing the liquid volume in the wells, the volume of air bubbles and their periodicity. With a well-filling volume of 150 µl, well-to-well contamination was successfully avoided by leaving a break time of 1 min between air bubbles of 30 µl.

Once the stress test parameters were set up, Antigen 18A aggregation kinetics upon air bubbling was followed in the microplate by tryptophan fluorescence and ultraviolet absorption. No change in turbidity was noticed, as evaluated by optical density measurement at 350 nm. In parallel with these label-free methods, the aggregation profile was measured by size-exclusion chromatography.

A change in fluorescence intensity can be attributed to a conformational change only when the sample concentration

remains stable during the stress test. However, during air bubbling, water evaporation or material loss by adsorption on tips may occur. As a consequence, well-to-well variations in protein concentration may lead to misinterpretations of tryptophan fluorescence data, and this should be avoided. The interchangeability of ultraviolet absorption and tryptophan fluorescence for measuring the concentration of native Antigen 18A was first verified (Fig. 5). It was also observed that absorption spectroscopy is a more reliable method than fluorescence spectroscopy for determining protein content in the presence of aggregated species (data not shown). Indeed, absorption is a faster process than fluorescence; it is less sensitive to solvent polarity hence to protein conformation (29). Therefore, the concentration dependence of tryptophan fluorescence was suppressed by normalizing all results with protein concentration determined by ultraviolet absorption (39). Both measurements were successively performed on each well in the same microplate reader.

Antigen 18A aggregation state was reproducibly controlled by adapting the number of air bubbles used in the test (Fig. 6a). A good correlation was observed between monomer detected by SEC and tryptophan fluorescence intensity (Fig. 6b). In order to have a reasonable stress test with an acceptable variability, we decided to set up the number of air bubbles at 100, corresponding to 44±2% monomer loss.

High-Throughput Screening of Excipients

The development of the microplate-adapted stress test for studying Antigen 18A aggregation at air-liquid interface made possible an HTS of excipients by tryptophan fluorescence spectroscopy.

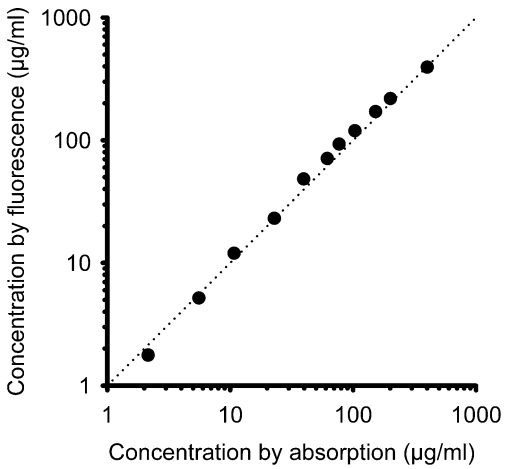

Fig. 5 Comparison of ultraviolet absorption spectroscopy and tryptophan fluorescence spectroscopy in determining the concentration of native Antigen 18A in microplate.

A panel of 44 excipients was investigated. Since an HTS approach allows the testing of a large number of conditions, this selection encompassed compounds from various chemical natures, independently of their described mode of action. The only selection criterion of an excipient was its presence in at least one marketed parenteral product. The working concentrations of excipient families were based on their usual injectability range. However, some amino acids (aspartic acid, glutamic acid, leucine and isoleucine) were tested at lower concentrations due to solubility issues at the target pH (6.8) of the study. Before screening, no interference of excipient stock solutions was noticed by both ultraviolet absorption and tryptophan fluorescence.

The performance of these 44 excipients was evaluated in triplicate at six different concentrations. The entire screening consisted of 12 plates in which all conditions were randomized. Excipient-free controls were present on each plate. More details can be found in the Materials and Methods section.

Sample preparation was performed with an automated liquid handler. Each plate was analyzed, submitted to air bubbling, centrifuged and analyzed again. A customized application was designed for data management and analysis. For each well, sample concentration was obtained from ultraviolet absorption spectroscopy. In excipient-free controls, we observed a decrease in protein concentration of 36±9% due to air bubbling, even if 30±4% water evaporation (30) was measured. We hypothesize that protein loss occured by adsorption on tips or on the walls of microplate wells. In the presence of excipients, a decrease in protein concentration was noticed in 42% of the wells, suggesting that 58% of these conditions inhibited protein loss by adsorption. The change in tryptophan fluorescence intensity normalized for concentration was then computed (F/F_0). This parameter was used for evaluating protein conformational change upon air bubbling in the presence of excipients. Based on an ANOVA followed by a Dunnett test ($\alpha=0.01$), a statistical module automatically evaluated if each condition (three samples) was significantly different from excipient-free controls (72 samples).

Results of the screening are presented in Fig. 7. The conditions where significant protection or destabilization of Antigen 18A was observed are labelled with black-filled or grey-filled symbols, respectively. Interestingly, different patterns were observed when studying the effect of excipient concentration on tryptophan fluorescence intensity. For instance, a linear increase was obtained for hydroxypropyl-cyclodextrins, a bell-shaped curve for poloxamers and a U-shaped curve for polyvinylpyrrolidones.

Among the 44 excipients evaluated, hit compounds were selected based on the following criteria: at least two consecutive concentrations significantly protected Antigen 18A from aggregation at air-liquid interface,

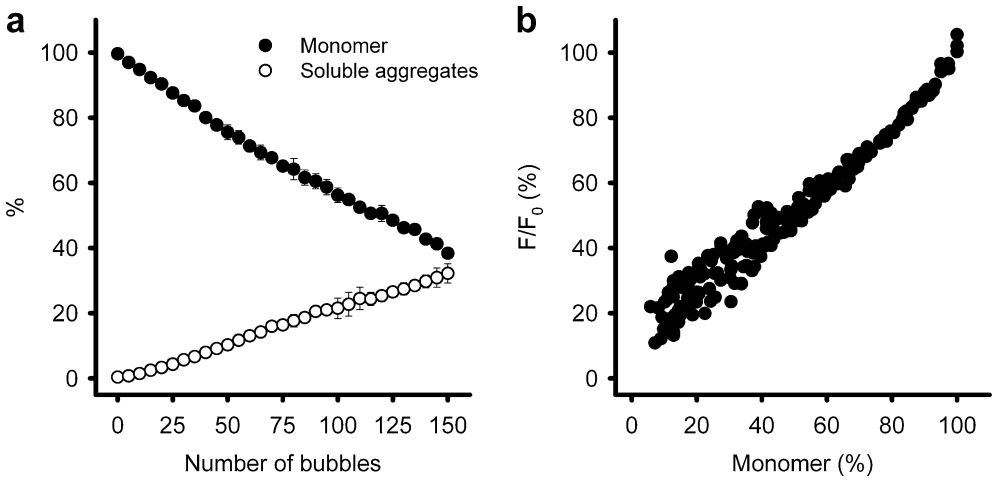

Fig. 6 Influence of air-liquid interface on Antigen 18A aggregation profile by size-exclusion chromatography and tryptophan fluorescence spectroscopy. Air-liquid interface was created by air bubbling in microplate. (**a**) Evolution of monomer and soluble aggregate species upon air bubbling. *Error bars* represent the standard deviation from three independent experiments. (**b**) Comparison of size-exclusion chromatography and tryptophan fluorescence spectroscopy for measuring Antigen 18A stability.

and at least one of them had a F/F_0 value greater than 80%. Hit excipients were the seven following compounds: hydroxypropyl-β-cyclodextrin, hydroxypropyl-γ-cyclodextrin, poloxamers 188 and 407, polysorbates 20 and 80, and Myrj 52. No significant effect of any hit excipient on pH was observed ($p>0.01$).

Based on the 72 excipient-free controls, the repeatability (intraplate), reproducibility (interplate) and global variability (intraplate + interplate) were estimated to be 12%, 7% and 13%, respectively. No significant row or column effect was observed ($p>0.01$).

In order to evaluate the feasibility of identifying hit excipients by this HTS method, we calculated a z'-value post-screening. This adimensional statistical parameter gives an idea of the width of the screening window (34). From the screening results (Fig. 7), we selected the positive (PX 188 0.125%) and negative (PVP K17 0.25%) controls based on a significant protection or destabilization of Antigen 18A at air-liquid interface, respectively. A plate was filled with positive and negative controls, in the same configuration as in the screening, i.e. blanks were placed on outer rows and all conditions were randomized on the plate. The samples were then submitted to air bubbling. Results are presented on Fig. 8. We obtained the following F/F_0 results: 94±2% for positive controls and 59±3% for negative controls. The calculated z'-value was 0.57, making the identification of excipient hits by this HTS method feasible (34).

Confirmation of the Performance of Hit Excipients

The performance of the seven hit excipients was further studied in half-filled vials. A shaking time of 1 h 30 min was applied (44±6% monomer loss) in order to meet conditions similar to the 100 bubbles used in the HTS study (44±2% monomer loss). Results of SEC analyses are presented in Fig. 9a. Significant protection of Antigen 18A ($p<0.05$) was observed with both cyclodextrins at 10% and with all surfactants from 0.015%.

Based on SEC results, a concentration of 10% for hydroxypropylcyclodextrins and 0.015% for surfactants was selected for further characterization. ELISA was used to assess the integrity of Antigen 18A epitopes after 1 h 30 min of shaking in vials in the presence of excipient candidates. Results are presented in Fig. 9b. After 1 h 30 min of shaking, hydroxypropylcyclodextrins and poloxamers significantly protected Antigen 18A from aggregation at air-water interface ($p<0.05$).

DISCUSSION

Aggregation in the Presence of Air-Liquid Interface

SEC analyses showed a progressive degradation of Antigen 18A monomer and the formation of soluble aggregates upon shaking in a half-filled vial (Fig. 1) or submission to air bubbles in a microplate (Fig. 6a). In both stress conditions, a simple mass balance calculation showed a progressive decrease in protein recovery. A loss of protein material could be explained by the presence of insoluble aggregates that are not detected by size-exclusion chromatography. This hypothesis is supported by a total disappearance of monomer and soluble aggregate species by SEC with harsher shaking protocols even if no particle was detected by visual observation (data not shown). While SEC is often considered as the standard reference for studying protein aggregation, this separation technique has potential limitations, e.g. interactions with stationary phase, modifications of the aggregate profile due to pressure or sample dilution, and loss of large particles on the chromatographic resin by filtration (40).

Spectroscopic and light scattering techniques were used to characterize Antigen 18A aggregation kinetics when

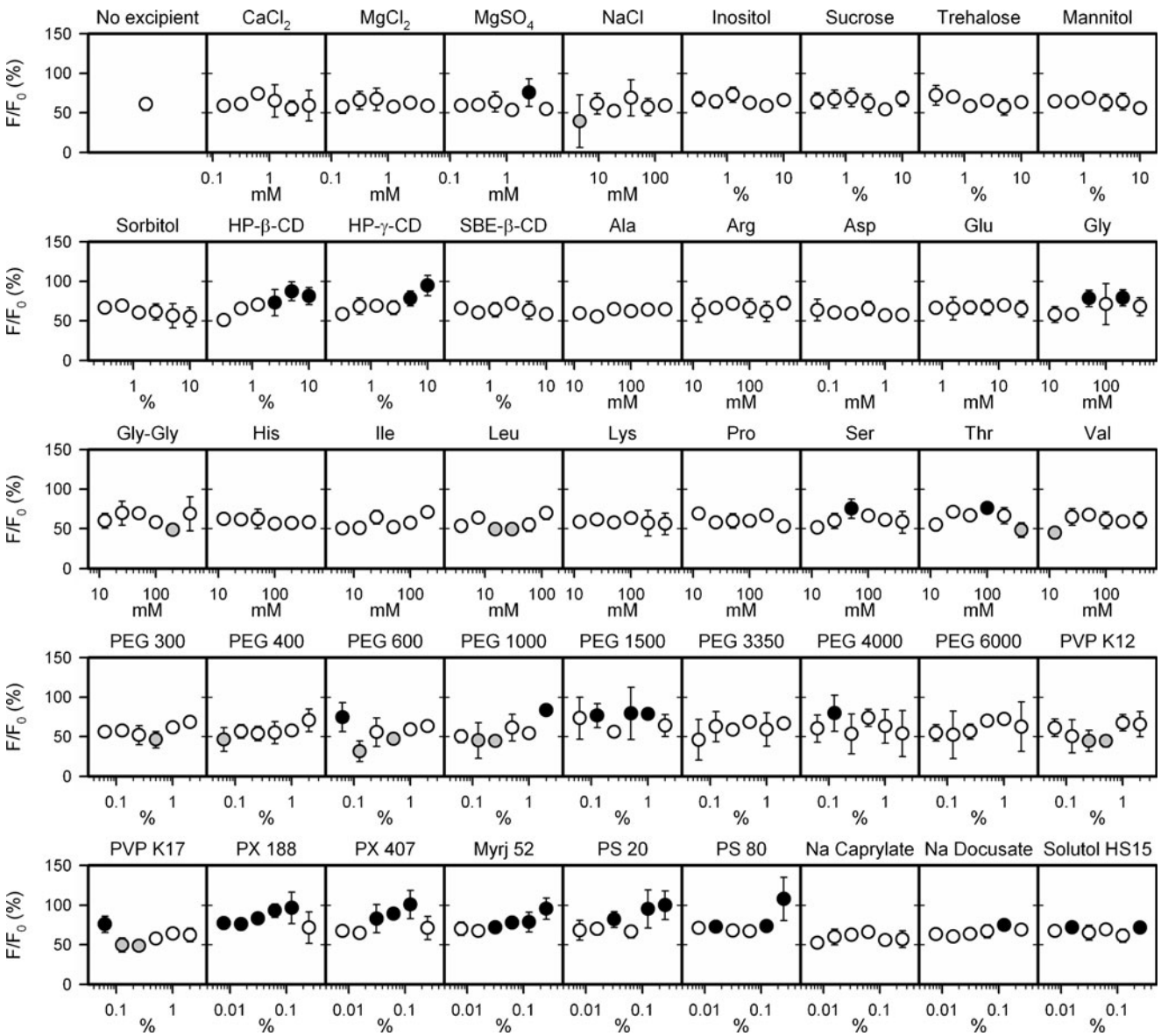

Fig. 7 High-throughput screening of excipients to prevent Antigen 18A aggregation at air-liquid interface, followed by tryptophan emission at 336 nm. A total of 100 air bubbles were used for creating air-liquid interface in microplate wells. *Closed symbols* represent conditions where statistically significant protection (*black*) or destabilization (*grey*) was noticed ($p < 0.01$) by ANOVA-Dunnett analysis. *Error bars* represent the standard deviation from three replicates randomly located on different plates.

shaken in a half-filled vial. Upon shaking, we measured an increase in β-sheet content (ATR-FTIR, Fig. 4), in the exposure of hydrophobic regions (Nile Red fluorescence spectroscopy, Fig. 3), and in aggregation (OD_{350} and RALS, Fig. 2).

Among all methods used in this aggregation kinetics study, Nile Red fluorescence revealed to be the most sensitive technique. By monitoring the position of the center of gravity of emission, we observed a significant increase in protein surface hydrophobicity after 30 min of shaking (Fig. 3c). Analyses by SEC were performed in parallel, and aggregation was significantly observed after 1 h of shaking. Nile Red fluorescence was already reported to have a higher sensitivity than SEC (36). The less discriminative techniques were light scattering methods. Aggregates were significantly detected after 2 h 15 min of shaking by RALS (Fig. 2a) and 3 h 30 min of shaking by OD_{350} (Fig. 2b). The superiority of RALS on OD_{350} could be due to the detector position. Whereas the latter is a transmission method, the detector is located at 90° in the former, which is more convenient for turbidity measurements.

These data suggest that conformational changes are involved in Antigen 18A aggregation at air-liquid interface. The use of complementary biophysical techniques was shown to be necessary for the characterization of protein aggregates (40). Indeed, while similar SEC profiles (Fig. 1a)

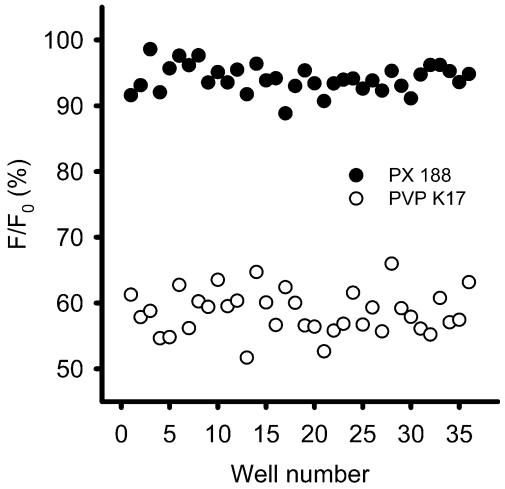

Fig. 8 Post-screening validation of the high-throughput screening assay. Controls were selected based on the HTS results, where significant protection (poloxamer 188 0.125%) or destabilization (polyvinylpyrrolidone K17 0.25%) of Antigen 18A against aggregation at air-liquid interface was noticed. Results were obtained from a single microplate.

were observed for aggregates obtained by shaking in a half-filled vial or by air bubbling in a microplate, fluorescence spectroscopy was able to detect some differences. For instance, tryptophan fluorescence spectroscopy detected significant changes upon air bubbling (Fig. 6b), while no differences were obtained upon shaking (data not shown). The opposite was true with Nile Red that detected significant differences upon shaking (Fig. 3) but not upon air bubbling (data not shown). Therefore, it was necessary to evaluate the performance of excipient candidates in both types of stress conditions.

High-Throughput Screening of Excipients

Early development of a vaccine formulation is often driven by a low availability of antigen material and short deadlines. Therefore, in a classical development, the number of excipients evaluated is limited. Surfactants are classically used in order to prevent protein adsorption at air-liquid interface and the resulting aggregation (10,12,16–23). In addition, a couple of studies report protein stabilization by adapting the formulation pH (7,9) or by adding excipients, e.g. cyclodextrins (10,15,19,24), amino acids (7–9), or sugars (6). Therefore, competition at interfaces but also conformational and colloidal stabilization can play a role in preventing protein aggregation at air-water interface.

HTS technologies are based on fast analyses and low sample volumes. A large number of conditions can be tested with a relatively small amount of antigen material. Moreover, each condition can be replicated in order to integrate a statistical approach in data interpretation. The excipients evaluated in this study were first selected based on their presence in marketed drugs for the parenteral route. While there is an urgent need for identifying new excipients from an academic point of view (41), using approved excipients limits development time by avoiding long and costly toxicological studies. Some excipient families were not included in this study, as their use was considered out of scope, e.g. antioxidants and preservatives. Also, some compounds were discarded in view of the adverse effects with which they are associated, considering that vaccines are most of the time used in a prophylactic context and intended to neonates. Finally, a non-exhaustive

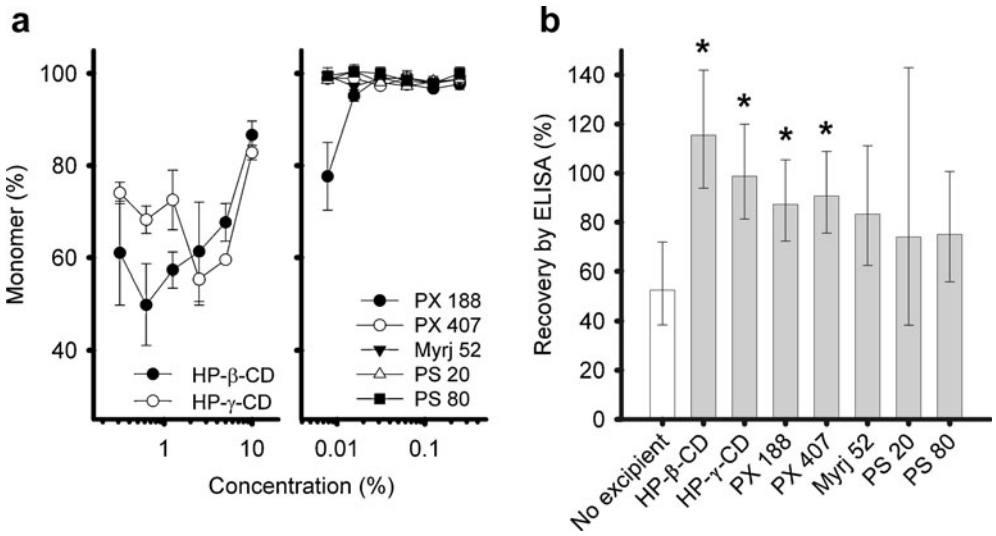

Fig. 9 Confirmation of the performance of excipient candidates in a shaken vial model. Agitation was performed during 1 h 30 min. (**a**) Monomer recovery by size-exclusion chromatography. *Error bars* represent the standard deviation from 3 independent experiments. (**b**) Integrity of Antigen 18A epitopes by enzyme-linked immunosorbent assay. Cyclodextrins and surfactants were added at a concentration of 10% and 0.015%, respectively. *Histogram bars* represent geometric means and their 95% confidence interval from five independent measurements. *Star symbols* indicate significant difference with the excipient-free control ($p < 0.05$) by ANOVA-Dunnett analysis.

list of 44 excipients was established, compatible with the liquid handler robot configuration used in this study. This excipient selection is convenient for studying the aggregation of a protein antigen irrespective of protein nature and stress test applied. We verified that the selected excipients did not interfere with the analytical methods used in this study.

The high sensitivity of fluorescence techniques (29) makes them very convenient to work at the low protein concentrations found in vaccines (typically lower than 1 mg/ml). Tryptophan fluorescence spectroscopy is a non-separative and label-free method, i.e. the sample is analyzed as such and no preparation is required. This technique was shown to be convenient for following Antigen 18A aggregation at 125 µg/ml (Fig. 6b). Combining tryptophan fluorescence spectroscopy with ultraviolet absorption spectroscopy in a multimode microplate reader allowed us to reliably measure the conformational changes of Antigen 18A in stress conditions and in the presence of various excipients (Fig. 7).

A major bottleneck in HTS is data management (26). While analyses are generally rapid, the thousands of figures generated by microplate readers can rapidly be overwhelming, and data management becomes a time-consuming operation. Each HTS process is different and requires the development of a customized application, based on the format of input and output files associated with equipments, plate layout, nature of analyses, calculations to be performed, and user requirements in terms of result display. In this study, we developed an integrated application used in the whole HTS process. Without any manual intervention from the generation of worklists used by the liquid handler robot up to the display of results, the risk of error was greatly reduced. Sample randomization in the plates increased objectivity. This approach allowed us to save time and to confidently interpret the HTS results.

The HTS evaluation of the 44 excipients revealed the performance of five surfactants and two cyclodextrins (Fig. 7). Protein protection by polysorbates (10,16–23), poloxamers (12) and hydroxypropylcyclodextrins (10,15,19,24) is already described in literature. Sulfobutylether-ethyl-cyclodextrin derivatives were also reported to have surfactant-like properties but were not included in this study because they are not used in any current commercial products (42). The amphiphilic nature of the surfactants but also of HP-β-CD (19) makes them good competitors for interfaces. These surface-active excipients could limit protein accessibility to air-water interfaces and therefore prevent adsorption-induced denaturation that triggers the aggregation process (2). A lower concentration of denatured species at interface may also limit irreversible interactions leading to the formation of aggregates. In addition, the protection conferred by an excipient could be possibly due to interactions with the protein (14,16) or to restriction in protein mobility due to an increase in viscosity. The question of protein stabilization mechanism by hit excipients was not addressed in this study. Using additional techniques including surface-tension and viscosity measurements would have been necessary for evaluating these different mechanistic approaches.

The critical micelle concentration (CMC) of a surfactant is the concentration from which micelles start to form. In absence of protein-surfactant interactions, protection by polysorbate 20 was reported to be maximal close to its CMC, independent of protein concentration (22). Another study showed protein stabilization by hydrophobic interactions with polysorbate 20 or 80 and protection below CMC, at surfactant:protein equimolar ratio (16). Therefore, both the nature of the surfactant and the nature of surfactant:protein interactions may play a role in protein protection from aggregation at air-liquid interface. As a rule of thumb, a monolayer of surfactant at interface should confer optimal protection, by using a concentration just above the excipient CMC (41). We observed that poloxamers 188 and 407 stabilized Antigen 18A at all concentrations, except the highest one (Fig. 7). A similar effect was shown to occur with polysorbate 80 (13). CMC values of 0.1% (25°C) and 0.095% (25.5°C) were found in literature for poloxamers 188 (43) and 407 (44), respectively. For both excipients, maximum protection was noticed at 0.125% ($p<0.01$), just above CMC, while no protection was observed at 0.250% ($p>0.01$). We postulate that Antigen 18A protection by poloxamers is concentration-dependent and that an optimum can be found close to the CMC.

Depending on the excipient:protein ratio, some additives revealed a beneficial or a detrimental effect on protein stability. Since the performance of an excipient can be related to its concentration, an HTS approach can be very convenient for simultaneously studying a large number of excipient:protein ratios. However, the efficient concentrations observed by tryptophan fluorescence in HTS (Fig. 7) were different from those observed by SEC in a shaken vial (Fig. 9a), probably due to differences in the nature of aggregates and to a lesser extent to the analytical method used (Fig. 6). These observations suggest that this HTS study of protein aggregation at air-liquid interface is convenient for identifying excipients but not for selecting excipient:protein ratios where the use of complementary biophysical techniques is required (40).

The performance of hydroxypropylcyclodextrins and poloxamers in protecting Antigen 18A from aggregation at air-liquid interface was confirmed in two different stress protocols. HP-β-CD at 0.35% was reported to be a valuable alternative to surfactants in inhibiting agitation-induced IgG aggregation (19). However, in the present study, adding 10% HP-β-CD or HP-γ-CD was necessary for observing a stabilizing effect on Antigen 18A, while aggregation was prevented by adding 0.015% poloxamer 188 or 407. At this concentration, a protective effect was

observed with poloxamers but not with polysorbates and Myrj 52 (Fig. 9b).

By identifying excipients known in the literature for stabilizing proteins against aggregation at air-liquid interface, the validity of the present HTS approach was confirmed. This objective strategy can find applications involving other analytical techniques, proteins and stress tests.

CONCLUSIONS

Antigen 18A was shown to denature in the presence of air-liquid interface and to form aggregates. We demonstrated the feasibility of identifying excipients for protecting this protein against aggregation at air-water interface by an HTS method. While amino acids, carbohydrates, polyols, polymers and salts appeared to be inefficient in that respect, some nonionic surfactants and hydroxypropylcyclodextrins were identified as performant excipient candidates. The superiority of poloxamers on polysorbates at protecting Antigen 18A was demonstrated.

Provided an integrated data management solution is available, HTS can be a powerful approach for evaluating the performance of excipients in protecting a protein antigen from aggregation. The high sensitivity of fluorescence methods makes them very convenient for working at low protein concentrations typical of vaccines. The case of Antigen 18A aggregation at air-liquid interface was presented but a similar HTS approach could be envisioned in other protein stability studies.

ACKNOWLEDGMENTS

This work was supported by GlaxoSmithKline Biologicals. The authors thank BASF, CyDex, Roquette and Sasol for providing gift samples of excipients, Laurent Bessemans and Caroline de Raikem for their support in programming the liquid handling robot, Carine Schroeders for technical assistance with ELISA analyses, Bénédicte Gbaguidi for advice with ATR-FTIR spectroscopy, the GlaxoSmithKline Biologicals R&D Media Preparation team for preparing excipient solutions, and Ulrike Krause and Pascal Cadot for their continuous support in reviewing the manuscript.

REFERENCES

1. Rathore N, Rajan RS. Current perspectives on stability of protein drug products during formulation, fill and finish operations. Biotechnol Prog. 2008;24(3):504–14.
2. Wang W. Protein aggregation and its inhibition in biopharmaceutics. Int J Pharm. 2005;289(1–2):1–30.
3. Hermeling S, Crommelin DJ, Schellekens H, Jiskoot W. Structure-immunogenicity relationships of therapeutic proteins. Pharm Res. 2004;21(6):897–903.
4. Hlady V, Buijs J, Jennissen HP. Methods for studying protein adsorption. Methods Enzymol. 1999;309:402–29.
5. Sluzky V, Tamada JA, Klibanov AM, Langer R. Kinetics of insulin aggregation in aqueous solutions upon agitation in the presence of hydrophobic surfaces. PNAS. 1991;88(21):9377–81.
6. Katakam M, Banga AK. Aggregation of insulin and its prevention by carbohydrate excipients. PDA J Pharm Sci Technol. 1995;49 (4):160–5.
7. Bringer J, Heldt A, Grodsky GM. Prevention of insulin aggregation by dicarboxylic amino acids during prolonged infusion. Diabetes. 1981;30(1):83–5.
8. Soenderkaer S, van de Weert M, Hansen LL, Flink J, Frokjaer S. Evaluation of statistical design/modeling for prediction of the effect of amino acids on agitation-induced aggregation of human growth hormone and human insulin. Drug Del Sci Tech. 2005;15:427–34.
9. Quinn R, Andrade JD. Minimizing the aggregation of neutral insulin solutions. J Pharm Sci. 1983;72(12):1472–3.
10. Charman SA, Mason KL, Charman WN. Techniques for assessing the effects of pharmaceutical excipients on the aggregation of porcine growth hormone. Pharm Res. 1993;10(7):954–62.
11. Maa YF, Hsu CC. Protein denaturation by combined effect of shear and air-liquid interface. Biotechnol Bioeng. 1997;54 (6):503–12.
12. Katakam M, Banga AK. Use of poloxamer polymers to stabilize recombinant human growth hormone against various processing stresses. Pharm Dev Technol. 1997;2(2):143–9.
13. Katakam M, Bell LN, Banga AK. Effect of surfactants on the physical stability of recombinant human growth hormone. J Pharm Sci. 1995;84(6):713–6.
14. Bam NB, Cleland JL, Yang J, Manning MC, Carpenter JF, Kelley RF, *et al.* Tween protects recombinant human growth hormone against agitation-induced damage via hydrophobic interactions. J Pharm Sci. 1998;87(12):1554–9.
15. Hagenlocher M, Pearlman R. Use of a substituted cyclodextrin for stabilization of solutions of recombinant human growth hormone. Pharm Res. 1989;6:S30.
16. Chou DK, Krishnamurthy R, Randolph TW, Carpenter JF, Manning MC. Effects of Tween 20 and Tween 80 on the stability of Albutropin during agitation. J Pharm Sci. 2005;94(6):1368–81.
17. Mahler HC, Muller R, Friess W, Delille A, Matheus S. Induction and analysis of aggregates in a liquid IgG1-antibody formulation. Eur J Pharm Biopharm. 2005;59(3):407–17.
18. Kiese S, Pappenberger A, Friess W, Mahler HC. Shaken, not stirred: mechanical stress testing of an IgG1 antibody. J Pharm Sci. 2008;97(10):4347–66.
19. Serno T, Carpenter JF, Randolph TW, Winter G. Inhibition of agitation-induced aggregation of an IgG-antibody by hydroxypropyl-beta-cyclodextrin. J Pharm Sci. 2010;99 (3):1193–206.
20. Thirumangalathu R, Krishnan S, Ricci MS, Brems DN, Randolph TW, Carpenter JF. Silicone oil- and agitation-induced aggregation of a monoclonal antibody in aqueous solution. J Pharm Sci. 2009;98 (9):3167–81.
21. Joshi O, Chu L, McGuire J, Wang DQ. Adsorption and function of recombinant Factor VIII at the air-water interface in the presence of Tween 80. J Pharm Sci. 2009;98(9):3099–107.
22. Kreilgaard L, Jones LS, Randolph TW, Frokjaer S, Flink JM, Manning MC, *et al.* Effect of Tween 20 on freeze-thawing- and agitation-induced aggregation of recombinant human factor XIII. J Pharm Sci. 1998;87(12):1597–603.
23. Wang W, Wang YJ, Wang DQ. Dual effects of Tween 80 on protein stability. Int J Pharm. 2008;347(1–2):31–8.

24. Banga AK, Mitra R. Minimization of shaking-induced formation of insoluble aggregates of insulin by cyclodextrins. J Drug Target. 1993;1(4):341–5.
25. Zhao H, Graf O, Milovic N, Luan X, Bluemel M, Smolny M, *et al.* Formulation development of antibodies using robotic system and High-Throughput Laboratory (HTL). J Pharm Sci. 2010;99 (5):2279–94.
26. Capelle MA, Gurny R, Arvinte T. A high throughput protein formulation platform: case study of salmon calcitonin. Pharm Res. 2009;26(1):118–28.
27. Ausar SF, Chan J, Hoque W, James O, Jayasundara K, Harper K. Application of extrinsic fluorescence spectroscopy for the high throughput formulation screening of aluminum-adjuvanted vaccines. J Pharm Sci. 2011;100(2):431–40.
28. Kyte J, Doolittle RF. A simple method for displaying the hydropathic character of a protein. J Mol Biol. 1982;157(1):105–32.
29. Lakowicz JR. Principles of fluorescence spectroscopy. New York: Springer; 2004.
30. McGown EL, Hafeman DG. Multichannel pipettor performance verified by measuring pathlength of reagent dispensed into a microplate. Anal Biochem. 1998;258(1):155–7.
31. Goormaghtigh E, Ruysschaert JM, Raussens V. Evaluation of the information content in infrared spectra for protein secondary structure determination. Biophys J. 2006;90(8):2946–57.
32. Kendrick BS, Dong A, Allison SD, Manning MC, Carpenter JF. Quantitation of the area of overlap between second-derivative amide I infrared spectra to determine the structural similarity of a protein in different states. J Pharm Sci. 1996;85 (2):155–8.
33. Oehlert GW. A first course in design and analysis of experiments. New York: W.H. Freeman & Co; 2000.
34. Zhang JH, Chung TD, Oldenburg KR. A simple statistical parameter for use in evaluation and validation of high throughput screening assays. J Biomol Screen. 1999;4(2):67–73.
35. Sackett DL, Wolff J. Nile red as a polarity-sensitive fluorescent probe of hydrophobic protein surfaces. Anal Biochem. 1987;167 (2):228–34.
36. Sutter M, Oliveira S, Sanders NN, Lucas B, van Hoek A, Hink MA, *et al.* Sensitive spectroscopic detection of large and denatured protein aggregates in solution by use of the fluorescent dye Nile red. J Fluoresc. 2007;17(2):181–92.
37. Byler DM, Susi H. Examination of the secondary structure of proteins by deconvolved FTIR spectra. Biopolymers. 1986;25 (3):469–87.
38. Dong A, Huang P, Caughey WS. Protein secondary structures in water from second-derivative amide I infrared spectra. Biochemistry. 1990;29(13):3303–8.
39. Pain RH. Determining the fluorescence spectrum of a protein. Curr Protoc Protein Sci. 2004;S38:7.7.1–7.7.20.
40. Carpenter JF, Randolph TW, Jiskoot W, Crommelin DJ, Middaugh CR, Winter G. Potential inaccurate quantitation and sizing of protein aggregates by size exclusion chromatography: essential need to use orthogonal methods to assure the quality of therapeutic protein products. J Pharm Sci. 2010;99(5):2200–8.
41. Jorgensen L, Hostrup S, Moeller EH, Grohganz H. Recent trends in stabilising peptides and proteins in pharmaceutical formulation - considerations in the choice of excipients. Expert Opin Drug Deliv. 2009;6(11):1219–30.
42. Samra HS, He F, Bhambhani A, Pipkin JD, Zimmerer R, Joshi SB, *et al.* The effects of substituted cyclodextrins on the colloidal and conformational stability of selected proteins. J Pharm Sci. 2010;99(6):2800–18.
43. Saski W, Shah SG. Availability of drugs in the presence of surface-active agents. I. Critical micelle concentrations of some oxyethylene oxypropylene polymers. J Pharm Sci. 1965;54:71–4.
44. Rassing J, Attwood D. Ultrasonic velocity and light-scattering studies on the polyoxyethylene-polyoxypropylene copolymer Pluronic F127 in aqueous solution. Int J Pharm. 1982;13(1):47–55.

ARTICLE

BIOTECHNOLOGY and BIOENGINEERING

High-Throughput Assessment of Antigen Conformational Stability by Ultraviolet Absorption Spectroscopy and Its Application to Excipient Screening

Sébastien Dasnoy,[1] Vivien Le Bras,[2] Véronique Préat,[1] Dominique Lemoine[2]

[1]Louvain Drug Research Institute, Pharmaceutics and Drug Delivery, Université catholique de Louvain, Brussels, Belgium

[2]GlaxoSmithKline Biologicals, Rue de l'Institut 89, 1330 Rixensart, Belgium; telephone: +32-2-656-6624; fax: +32-2-656-3222; e-mail: dominique.lemoine@gskbio.com

Received 14 June 2011; revision received 31 August 2011; accepted 6 September 2011

Published online 16 September 2011 in Wiley Online Library (wileyonlinelibrary.com). DOI 10.1002/bit.23336

ABSTRACT: In high-throughput screening (HTS) assays, the use of ultraviolet absorption spectroscopy (UA) is commonly limited to concentration and turbidity measurements. Our aim was to evaluate microplate-based UA and its second-derivative [(2d)UA] for measuring the conformational stability of two recombinant antigenic proteins in the presence of 44 excipients. Protein conformational stability was assessed by (2d)UA upon titration with guanidine hydrochloride. (2d)UA was compared with tryptophan fluorescence spectroscopy (TF) and differential scanning fluorimetry (DSF), both commonly used techniques for measuring protein conformational stability. The HTS data were corrected for plate, row and column effects by applying a median polish procedure. Irrespective of the unfolding method applied, similar stabilizing excipients were identified by all analytical methods for a given antigen. The native forms of both antigens were destabilized by arginine, hydroxypropyl-β-cyclodextrin, and sodium docusate, and were protected by polyols. The median polish correction improved the quality of the prediction models and the screening resolution. The higher sensitivities of TF and DSF compared with (2d)UA allowed the identification of a larger number of stabilizing excipients. However, similar screening resolutions (z'-factor > 0.8) were observed for 2dUA, TF, and DSF in a HTS of excipients applied to one of the antigens. Therefore, (2d)UA deserves more attention in HTS studies focused on protein conformational stability.

Biotechnol. Bioeng. 2012;109: 502–516.

KEYWORDS: ultraviolet absorption spectroscopy; high-throughput screening; protein; excipients; vaccine

Introduction

Various stress conditions may affect vaccine integrity during manufacturing and storage (Shire, 2009). Antigen integrity is a critical factor in the preservation of a vaccine's immunogenicity profile (Hermeling et al., 2004). Ensuring protein conformational stability may help to limit protein aggregation (Thirumangalathu et al., 2009; Wang, 2005) and oxidation (Thirumangalathu et al., 2007). High-throughput screening (HTS) methods offer the potential for the rapid identification of excipients able to stabilize the conformation of protein-based antigens.

Over recent decades, numerous studies on protein conformation have been performed with spectroscopic methods, for example, fluorescence and circular dichroism. An increasing number of HTS studies report the evaluation and identification of protein-stabilizing conditions by intrinsic (Capelle et al., 2009; Dasnoy et al., 2011) and extrinsic (Capelle et al., 2009) fluorescence, differential static light scattering and differential scanning fluorimetry (DSF; Senisterra and Finerty, 2009). In contrast, ultraviolet absorption spectroscopy (UA), although available in most laboratories, has been mainly relegated to measuring protein concentrations, turbidity, and enzymatic activity (Mach and Middaugh, 2011). In microplates, UA is often used to measure protein concentration at 280 nm (Zhao et al., 2010) and sample turbidity at 350 or 360 nm (Ausar et al., 2007; Capelle et al., 2009; Kissmann et al., 2008a,b).

Protein conformational stability has already been studied by UA and second-derivative UA [(2d)UA] in cell-based spectrophotometers (He et al., 2010; Kueltzo et al., 2000; Peek et al., 2007; Vessely et al., 2009). To our knowledge, (2d)UA is not commonly used for studying protein conformational stability in microplates.

Correspondence to: Dominique Lemoine

Contract grant sponsor: GlaxoSmithKline Biologicals

Chemical (Aucamp et al., 2005; Liu et al., 2009) and thermal (Kueltzo et al., 2000; Peek et al., 2007; Senisterra and Finerty, 2009) unfolding methods have been used for measuring protein conformational stability. Both approaches were reported to have provided similar insights on protein thermodynamic stability (Pace and Scholtz, 1997).

Antigen A and Antigen B are experimental recombinant proteins for vaccination and produced by GlaxoSmithKline Biologicals (Rixensart, Belgium). The objective of this work was to demonstrate that (2d)UA can be used to study the effect of excipients on protein conformational stability in HTS mode. The chemical unfolding of Antigens A and B was monitored by various features extracted from (2d)UA spectra. Tryptophan fluorescence spectroscopy (TF) and DSF were used as benchmark analytical methods. The stabilizing excipients identified by (2d)UA, TF, and DSF were assessed in their ability to enhance the isothermal stability of the antigens.

Materials and Methods

Materials

Antigens A and B were produced by GlaxoSmithKline Biologicals. Both proteins were studied at a concentration of 250 μg/mL. Antigen A was prepared in 10 mM phosphate buffer (NaH_2PO_4/K_2HPO_4), pH 6.8. Antigen B was prepared in 10 mM tris(hydroxymethyl)aminomethane (Tris) buffer, pH 7.5, 10 mM NaCl.

L-Arginine (Arg), L-aspartic acid (Asp), L-histidine (His), L-isoleucine (Ile), L-leucine (Leu), L-proline (Pro), L-serine (Ser), L-threonine (Thr), and L-valine (Val) were obtained from Ajinomoto (Tokyo, Japan). L-Alanine (Ala) was obtained from Amresco (Solon, OH) and L-glycine (Gly) from Evonik Rexim (Ham, France). Polyethyleneglycol 15 hydroxystearate (*Solutol® HS15*), polyvinylpyrrolidones (PVP) K12 and K17 (*Kollidon®*), poloxamers (PX) 188 and 407 (*Lutrol®*) were gifts from BASF (Ludwigshafen, Germany). D-Mannitol was obtained from Roquette (Lestrem, France), D-sorbitol from Cargill (Minneapolis, MN), sucrose from VWR (West Chester, PA), polysorbate (PS) 80 from NOF (Tokyo, Japan), and hydroxypropyl-γ-cyclodextrin (HP-γ-CD, *Cavasol® W8 HP*) from Wacker (Burghausen, Germany). Hydroxypropyl-β-cyclodextrin (HP-β-CD, *Kleptose® HPB*) was a gift from Roquette. Sulfobutylether-β-cyclodextrin (SBE-β-CD, *Captisol®*) was a gift from CyDex Pharmaceuticals, Inc. (Lenexa, KS). Polyoxyl 40 stearate (Myrj 52) was obtained from Croda (Goole, UK). Sodium dioctylsulfosuccinate (sodium docusate) was purchased from Cytec (Woodland Park, NJ). Trehalose was obtained from Ferro Pfanstiehl (Waukegan, IL). Calcium chloride, magnesium chloride, magnesium sulphate, guanidine hydrochloride (Gdn.HCl), Tris, potassium hydrogenophosphate, ethanol, PS 20, sodium caprylate, polyethylene glycols (PEG) 300, 600, 1,000, 1,500, and 6,000 were obtained from Merck (Darmstadt, Germany). PEGs 400, 3,350, and 4,000 were gifts from Sasol (Johannesburg, South Africa). L-Glutamic acid (Glu), glycylglycine (GlyGly), L-lysine (Lys), *myo*-inositol, silicon oil (DC200, Fluka), 8-anilino-1-naphtalene-sulfonic acid (ANS), 4,4′-dianilino-1,1′-binaphthyl-5,5′-disulfonic acid dipotassium salt (bis-ANS), SYPRO Orange (SO), dimethylsulfoxide (DMSO), and sodium dihydrogenophosphate were obtained from Sigma–Aldrich (St. Louis, MO). All solutions were prepared with water for injection obtained by triple distillation. Excipient solutions were filtered through a 0.22 μm polyether sulfone membrane (Sartolab, Sartorius Stedim, Aubagne, France). All excipients except GlyGly were of compendial grade or tested following their respective Ph.Eur. monograph prior to use. Excipient concentrations are presented as percentages and were prepared on a weight-to-volume (w/v) basis.

Regular (Costar #3635) and half-area ultraviolet (UV)-transparent (Costar #3679) 96-well acrylic microtiter plates were obtained from Corning (Corning, NY), clear and black 96-well polypropylene microplates (Whatman Uniplate) were obtained from GE Healthcare (Waukesha, WI), and 384-well microplates (4titude Framestar 384) were obtained from Bioké (Leiden, The Netherlands). UV-transparent seals (VIEWseal) were obtained from Greiner Bio-one (Kremsmünster, Austria). *MicroAmp®* optical 96-well reaction plates and optical adhesive films were obtained from Life Technologies (Applied Biosystems, Carlsbad, CA).

Chemical Unfolding

Chemical unfolding was monitored by (2d)UA and TF. The titration method was adapted from Aucamp et al. (2005). Gdn.HCl stock solutions were prepared at a concentration of 5.0 M for Antigen A and 2.5 M for Antigen B. The initial sample volume was 75 μL. During the selection of conditions to monitor unfolding, empty wells were filled with water. Titration by Gdn.HCl was directly performed in a Varioskan Flash microplate reader (ThermoFisher Scientific, Waltham, MA) equipped with an automated dispenser. Various denaturant volumes were added during titration to explore the whole range of Gdn.HCl concentrations, to a final volume of 300 μL. After every addition of denaturant, the microplate was shaken during 30 s at 300 rpm, left during 5 min, analyzed by (2d)UA and then by TF. In preliminary experiments, we verified that repeated sample excitation by fluorescence did not affect absorption measurements. Each screening comprised twelve 96-well microplates, 30 additions of Gdn.HCl per well, and thus involved the recording of 34,560 UA spectra, sets of UA values or TF intensity values.

The microplate reader SkanIt software (ThermoFisher Scientific) was only used for data acquisition. Raw data were exported as text files. Data processing was performed by a customized application (Microsoft, Redmond, WA) developed in Visual Basic, with a SigmaPlot (Systat Software, San Jose, CA) embedded module for curve-fitting operations.

Chemical unfolding studies were performed assuming the equilibrium state in spectroscopic measurements and a two-state protein unfolding mechanism. Data points were fitted to a Boltzmann sigmoid function (Eq. 1), where D is the denaturant concentration, Y the signal, D_m the denaturant concentration at mid-transition, Y_n the signal of native protein, Y_u the signal of unfolded protein, and k the transition slope. Y_n, Y_u, D_m, and k were considered as floating parameters in the curve-fitting algorithm.

$$Y = Y_n + \frac{Y_u - Y_n}{1 + e^{\left(\frac{D_m - D}{k}\right)}} \quad (1)$$

The D_m parameter was selected for evaluating the conformational stability of protein antigens (Aucamp et al., 2005).

UV Absorption Spectroscopy

Spectroscopic measurements were performed at 25°C in unsealed UV-transparent microplates with a Varioskan Flash microplate reader (ThermoFisher). Spectra were recorded from 220 to 350 nm with a wavelength step of 1 nm, a bandwidth of 5 nm and an integration time of 100 ms. A microplate was scanned in 30 min. The sample turbidity before titration ($OD_{350} = 2.1 \pm 4.4$ mAU, after buffer subtraction) was too low for assessing the effect of excipients on protein stability.

Spectral processing is illustrated in Figure 1a. Since a more concave meniscus is observed in a protein-containing well than in a well filled with its associated buffer, the pathlength obtained for the protein well (L) is shorter than its blank counterpart (L'). Absorption values should be measured with the same pathlength to be compared. The Lambert–Beer law can be applied to absorbing species and states that absorption is directly proportional to pathlength, provided measurements are performed in the linear range of the detector. An absorption measurement A performed with a pathlength L can therefore be normalized to A' associated with L', according to Equation (2).

$$A' = \left(\frac{L'}{L}\right)A \quad (2)$$

The Lambert–Beer equation is not applicable to optical density (OD) values measured in a region where proteins do not absorb ($\lambda > 305$ nm). A pathlength correction in this region does not have any physical meaning. However, the pathlength correction does not modify the signal slope used in the light scattering correction applied in the next step.

Pathlength correction was applied to all measurements. The pathlength value was obtained by measuring the intensity of water absorption peak in the near-infrared region at 975 nm, from which the baseline intensity at 900 nm is subtracted (Dasnoy et al., 2011; McGown and Hafeman, 1998). The buffer to protein pathlength ratio (L'/L) gradually decreased during the Gdn.HCl titration, from 1.11 ± 0.20 to 0.95 ± 0.15 in the presence of excipients.

The buffer signal was subtracted. Buffer-corrected spectra were corrected for light scattering by extrapolating to shorter wavelengths the linear regression of the logarithm of OD as a function of the logarithm of wavelength (λ) in the 320–350 nm region, based on Equation (3) (Leach and Scheraga, 1960).

$$\log(OD) = a \log(\lambda) + b \quad (3)$$

The absorption values at 230 (Liu et al., 2009) and 290 nm (Thomson et al., 1989) were extracted and corrected for the protein concentration as determined by absorption at 280 nm. The wavelength at maximum of absorption in the 260–290 nm range (λ_{max}) and the wavelength at minimum of absorption in the 250–270 nm range (λ_{min}) were calculated by interpolation: a series of 19 points were added between raw data points, with a fifth-degree polynomial least-square fit. The center of gravity of absorption ($\langle\lambda\rangle$) was calculated in the 245–305 nm range by the center of spectral mass position ($\overline{\nu}_{csm}$) method (Eq. 4). Bandpass correction was applied when converting intensities (I) from wavenumbers ($\overline{\nu}$) to wavelength units (Lakowicz, 2004).

$$\langle\lambda\rangle = \frac{1}{\overline{\nu}_{csm}} = \frac{\sum I(\overline{\nu})}{\sum \overline{\nu} I(\overline{\nu})} = \frac{\sum \lambda^2 I(\lambda)}{\sum \lambda I(\lambda)} \quad (4)$$

Second-derivative spectra were obtained by simultaneous numerical smoothing and differentiation of buffer- and light scattering-corrected spectra by a nine-points filter and second-degree Savitzky–Golay polynomial (Savitzky and Golay, 1964). A series of 19 points were added between raw data points, with a sixth-degree polynomial least-square fit (Kueltzo et al., 2000). The spectra were truncated and limited to the 250–305 nm region. The concentration dependence of the second-derivative signal (z) was suppressed by vector-normalization (Eq. 5).

$$z_{norm} = \frac{z}{\sqrt{\sum z^2}} \quad (5)$$

The position of peaks and shoulders was determined based on differentiation of the second-derivative signal (Fig. 1b). A window of 2.5 10^{-4} intensity units and 5 nm wavelength was applied for peak localization. The three main negative peaks were identified near 285 nm (Tyr/Trp, A), 295 nm (Trp, B), and 260 nm (Phe, C). Peak-to-valley intensity ratios were used to determine the relative exposure of aromatic amino acid residues. The A/B ratio has been reported to be an indicator of Tyr exposure (Ragone et al., 1984). The similarity of spectra (y) with the non-treated sample (x) was monitored by the correlation coefficient (r, Eq. 6, after translation of spectra to positive domain; Prestrelski et al., 1993) and the root mean square of differences (RMS, Eq. 7, where n is the number of data

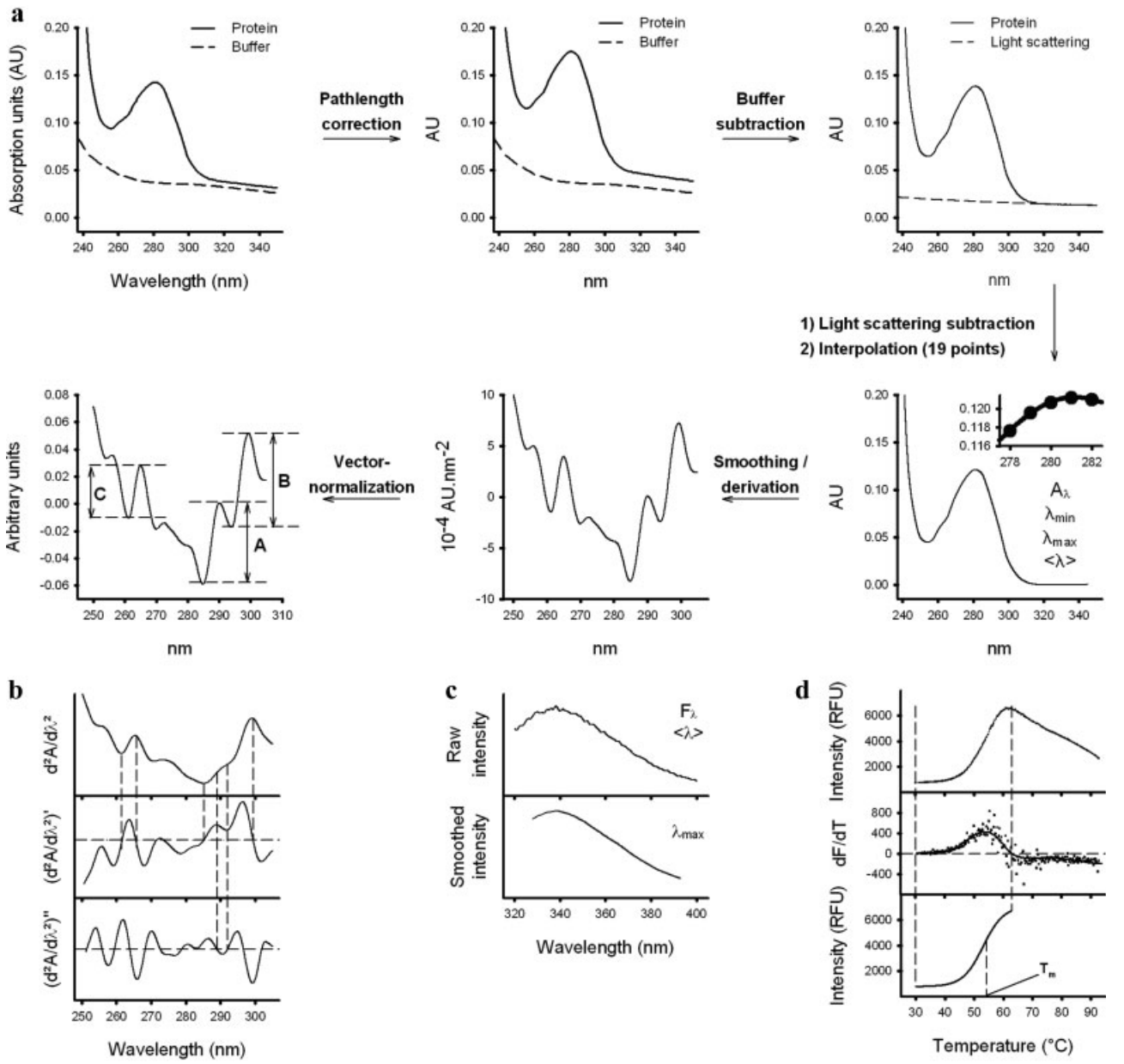

Figure 1. Signal processing in spectroscopic methods: (**a**) from UA to 2dUA spectra. After a pathlength correction performed by dividing OD values by $OD_{975} - OD_{900}$, the buffer signal was subtracted. The light scattering signal was calculated from the log-transformed 320–350 nm region according to Equation (3) and was subtracted. A least-square interpolation procedure added data points in the UA spectrum at wavelength increments of 0.05 nm. A Savitzky–Golay algorithm was used for calculating the 2dUA spectrum. The 2dUA spectrum was vector-normalized based on Equation (5), (**b**) determination of peak position in a 2dUA spectrum by differentiation, (**c**) Savitzky–Golay procedure used for smoothing a TF spectrum, (**d**) curve-fitting operations applied to DSF. The first-derivative smoothed with a moving average algorithm allows truncation of the signal to the transition region, subsequent curve-fitting and T_m extraction.

points; Park et al., 1989) methods.

$$r = \frac{\sum xy}{\sqrt{\sum x^2 \sum y^2}} \tag{6}$$

$$\mathrm{RMS} = \sqrt{\frac{\sum (x-y)^2}{n}} \tag{7}$$

In order to limit the time required for analysis, the scan window was shortened in excipient screening studies. For Antigen A, OD values were measured at 280 and 290 nm (normalized Trp absorption by OD_{290} to OD_{280} ratio), 900 and 975 nm (pathlength), and 320 and 350 nm (wavelength dependence of light scattering signal determined on two points, 3.3 min/plate). For Antigen B, absorption scans were recorded between 270 and 300 nm, and both pathlength and

light scattering were determined as explained for Antigen A (9.8 min/plate).

Tryptophan Fluorescence Spectroscopy

Spectroscopic measurements were performed at 25°C in unsealed UV-transparent microplates with a Varioskan Flash microplate reader (ThermoFisher Scientific). Selective excitation of Trp residues was performed at 295 nm (Lakowicz, 2004). Spectra were recorded from 320 to 420 nm, with a wavelength step of 1 nm, an excitation bandwidth of 12 nm and an integration time of 100 ms. A microplate was scanned in 21.4 min. Bottom optics were used because the focus position of the excitation beam was compatible with measurements in the whole volume range evaluated (75–300 μL). The buffer signal was subtracted. The center of gravity of the emission ($\langle\lambda\rangle$) of buffer-corrected spectra was calculated from Equation (4). The average emission of all Trp residues was monitored at 340 nm (F_{340}; Aucamp et al., 2005). The relative contribution of buried (emission at 330 nm) and exposed (emission at 350 nm) Trp residues was measured by ratio (F_{330}/F_{350}) and difference ($F_{330} - F_{350}$). The λ_{max} was extracted from buffer-corrected spectra after application of a 15-points filter and third-order Savitzky–Golay smoothing algorithm (Savitzky and Golay, 1964; Fig. 1c). TF has been used in a HTS study to evaluate the effect of excipients in their ability to prevent Antigen 18A from aggregation at air–water interface (Dasnoy et al., 2011). F_{340} was used in excipient screening for both antigens (1.6 min/plate).

Thermal Unfolding

Thermal unfolding was monitored by DSF. Measurements involving Antigens A and B were performed with a ABI Prism 7900HT sequence detection system (Life Technologies) and a LightScanner Pro (Idaho Technologies, Inc., Salt Lake City, UT), respectively. The selection of extrinsic fluorescent probes was based on a preliminary comparison of different dyes (data not shown). For Antigen A, 1 μL SO 250× in DMSO was added to 49 μL sample in *MicroAmp*® optical 96-well reaction plates sealed with *MicroAmp*® optical adhesive films. For Antigen B, each well of a parent 96-well polypropylene clear microplate was filled with 99 μL sample to which 1 μL of an ethanolic solution of ANS 500 μM was added. All wells of a daughter 384-well microplate were prefilled manually with 3 μL silicone oil for preventing evaporation during thermal unfolding (Antigen B). A 96-channel (TeMo) head (Tecan, Männedorf, Switzerland) was then used to transfer 10 μL from a parent well to each of four daughter wells. The daughter microplate was then sealed. Just before analysis, the microplate was centrifuged for 5 min at 2,500 rpm. Temperature was raised from 25 to 90°C, at a rate of 1°C/min.

Fluorescence intensity measurements were performed at 0.29 ± 0.06°C for Antigen A and 0.076 ± 0.002°C intervals for Antigen B. The softwares of both DSF systems were used for data acquisition only. Raw data were exported as text files and analyzed with customized Visual Basic macros (Microsoft). No buffer subtraction was performed. Data were automatically truncated to the transition region, based on the first-derivative smoothed with a running average algorithm (embedded SigmaPlot module; Fig. 1d). The obtained region was fitted to a Boltzmann sigmoid function (Eq. 8), where T is the temperature, Y the signal, T_m the temperature at mid-transition, Y_n the signal of native protein, Y_u the signal of unfolded protein, and k the transition slope. Y_n, Y_u, T_m, and k were considered as floating parameters in the curve-fitting algorithm.

$$Y = Y_n + \frac{Y_u - Y_n}{1 + e^{\left(\frac{T_m - T}{k}\right)}} \quad (8)$$

The T_m parameter was selected for evaluating the conformational stability of protein antigens. In the case of Antigen B, the values of the four daughter wells were averaged. The measurement was considered as invalid if no transition was observed or a transition was detected in the same temperature range as detected in the placebo formulation.

High-Throughput Screening of Excipients

The present HTS design has been used to evaluate excipients in their ability to protect Antigen 18A from aggregation at air–water interface (Dasnoy et al., 2011). Briefly, a series of 44 excipients were selected based on their presence in marketed parenteral drugs. Excipients were tested at six concentrations in triplicate. Replicates were located on different plates. Edge rows were used for placebo formulations. An excipient-free control was present on each row of a plate. The positions of all other test conditions were randomized in a total of 12 plates.

All samples contained 10 mM phosphate buffer (NaH_2PO_4/K_2HPO_4), pH 6.8 (Antigen A), or 10 mM Tris buffer, pH 7.5 (Antigen B). The stock solution concentrations were the following: 100 mM phosphate buffer, 0.5% surfactants, 3% polymers, 15% polyols except 12% inositol, 15% carbohydrates and cyclodextrins, 100 mM calcium and magnesium salts, 250 mM sodium chloride, 3 mM aspartic acid, 50 mM glutamic acid, 150 mM leucine, 250 mM isoleucine, and 500 mM other amino acids.

A customized application developed in Visual Basic (Microsoft) randomized the positions of all test conditions and generated XML worklists containing liquid volumes to be added in each well. This application subsequently imported XML worklists into the Gemini software (Tecan). A Genesis liquid handling station equipped with an eight-tip liquid handling (LiHa) arm (Tecan) prepared excipient mixes at a volume of 1,000 μL in deepwell microplates. In parallel, a deepwell plate containing antigen stock solution was prepared by hand. The transfer from deepwell to

microtiter plates was performed with the TeMo equipped with disposable tips (Tecan). Formulations were prepared in stock clear polypropylene microplates (200 μL) obtained by mixing appropriate volumes from excipient and antigen deepwell plates. The maximum final concentrations of excipients were the following: 0.25% surfactants, 2% polymers, 10% polyols, carbohydrates, and cyclodextrins, 50 mM calcium and magnesium salts, 150 mM sodium chloride, 2 mM aspartic acid, 25 mM glutamic acid, 120 mM leucine, 200 mM isoleucine, and 400 mM other amino acids. For a given excipient, the six concentrations studied were obtained as consecutive twofold dilutions from its maximum final concentration. The pH of final formulations was not measured.

Two microtiter plates were prepared with the TeMo from a stock microplate: a regular UV-transparent plate for chemical unfolding (75 μL), and another plate for DSF as explained in the Thermal Unfolding Section.

Isothermal Stability

Isothermal unfolding studies were performed at 45°C in a Varioskan Flash microplate reader (ThermoFisher Scientific). This temperature was selected as the highest allowed by the microplate reader software, SkanIt. Turbidity measurements were performed by OD at 350 nm in half-area UV-transparent microplates (Corning) filled with 150 μL of dye-free sample. Extrinsic fluorescence measurements were performed by assing a dye was chosen from preliminary experiments (data not shown). One microliter of a 500 μM bis-ANS (Antigen B) or a 500× SO (Antigen A) stock solution in DMSO was added to 99 μL of sample in a black microplate. The excitation/emission wavelengths of bis-ANS and SO were 385/525 and 490/600 nm, respectively. The dye was excited with a bandwidth of 12 nm, and emission was measured with an integration time of 100 ms.

Statistical Analysis

Data Correction

The data correction method was adapted from Malo et al. (2010), in an Excel spreadsheet (Microsoft). Briefly, a non-control-based normalization method was applied, aiming to reduce the noise introduced by the repartition of the experimental conditions on the twelve 96-well plates. Indeed, even though the test conditions are randomly located on the plates, without using the first and last rows, intra- and inter-plate effects may occur leading to false negative/positive results. A median polish procedure (Tukey, 1977) was applied. This method, well-suited to gridded data, works by alternately removing row and column medians from each plate, until all medians are nearly null. Because the outcome may vary slightly depending on whether rows or columns are considered first, both starting strategies were applied, with nine corrections cycles, and the obtained results averaged. Finally inter-plate differences were corrected by aligning the medians of all plates. Corrected results can be then calculated from Equation (9), corrected result for row i and column j on the pth plate $\left(\hat{x}_{ijp}\right)$ being the difference between the observed value $\left(x_{ijp}\right)$ and the corresponding predicted error $\left(\hat{\varepsilon}_{ijp}\right)$ calculated as the sum of row $\left(\hat{R}_{ip}\right)$, column $\left(\hat{C}_{jp}\right)$, and plate $\left(\hat{P}_{p}\right)$ biases.

$$\hat{x}_{ijp} = x_{ijp} - \hat{\varepsilon}_{ijp} = x_{ijp} - \left(\hat{R}_{ip} + \hat{C}_{jp} + \hat{P}_{p}\right) \tag{9}$$

Data Analysis

Corrected results were analyzed with Design Expert (Stat-ease, Minneapolis, MN) using a prediction approach. For each studied read-out, a global polynomial regression model was determined. This model is based on the combination of quadratic, linear, or absence of dose effect by excipient, aiming to predict as close as possible the observed responses, in a trustful way. To that end, several statistical criteria were used, like F-tests to check the significance of effects, the associated variance inflation factor (VIF) as a measure of the colinearity of coefficients, or the cross-validated coefficient of correlation between observations and predictions (Q^2). Then, for each excipient, the highest or lowest (depending on whether the excipient stabilizes or destabilizes the antigen) attainable response—in the tested concentration range—can be predicted, with its associated 95% confidence interval.

HTS Assay Validation

The z'-factor is a common adimensional parameter used for evaluating the quality of an HTS assay. Based on the mean (μ) difference and variability (σ) of positive ($C+$) and negative ($C-$) controls, a separation band was calculated (Dasnoy et al., 2011), according to Equation (10). The identification of hits by a HTS assay is considered as feasible when its z'-factor ≥ 0.5 (Zhang et al., 1999).

$$z' = 1 - 3\frac{(\sigma_{C+} + \sigma_{C-})}{|\mu_{C+} - \mu_{C-}|} \tag{10}$$

Results

The effect of a series of 44 excipients on the conformational stability of Antigens A and B was studied in HTS mode by (2d)UA, TF, and DSF. Protein unfolding was performed chemically (by using Gdn.HCl) for (2d)UA and TF, and thermally for DSF. Prior to excipient screening, the selection of the conditions for monitoring unfolding were undertaken for (2d)UA and TF.

Selection of Intrinsic Unfolding Probes

Proteins denature and unfold in the presence of Gdn.HCl. Various features were computed from (2d)UA and TF

spectra and evaluated to identify the settings to monitor unfolding through the use of (amino acid residue) probes intrinsic to the protein antigens. For Antigens A and B, features from the spectra associated with a sigmoid unfolding pattern were selected to generate a two-step unfolding model into which data were processed to extract D_m for estimating protein stability. It has been shown that when multiple features are extracted from a spectra, each of them can be associated with a different D_m value (Eftink, 2000).

UV Absorption Spectroscopy

In UA, a spectral shift to shorter wavelengths is accounted for by an increase in the polarity of the environment of aromatic amino acid residues, which may for instance be due to an increase in exposure to water. The peaks of aromatic amino acid residues contributing to a protein absorption spectrum (Phe/Tyr/Trp) can be resolved in the 2dUA spectrum (Kueltzo et al., 2000).

The evolution of (2d)UA spectra was analyzed upon unfolding by Gdn.HCl (Fig. 2a and b). The A_{230}/A_{280} (Fig. 2c) and A_{290}/A_{280} (Fig. 2d) ratios, λ_{max} (Fig. 2e), λ_{min} (Fig. 2f), and $\langle\lambda\rangle$ (Fig. 2g) positions extracted from UA spectra were monitored. Upon denaturant addition, the similarity of 2dUA spectra with the non-treated sample was assessed by the r (Eq. 6; Prestrelski et al., 1993; Fig. 2h) and the RMS (Eq. 7; Park et al., 1989; Fig. 2i) methods. The position (Fig. 2j–l) and peak-to-valley intensity ratios (Fig. 2m–o) of the three best-resolved aromatic amino acid peaks (A, B, and C) were monitored in 2dUA spectra.

Upon unfolding, blue shifts were detected for A_{290}/A_{280} (Fig. 2d), λ_{max} (Fig. 2e), λ_{min} (Fig. 2f), and A position (Fig. 2j). Some changes were detected in the relative exposure of amino acid residues, as evidenced by an increase in A/B (Fig. 2m) and A/C (Fig. 2n). No clear transition was observed for A_{230}/A_{280} (Fig. 2c), $\langle\lambda\rangle$ (Fig. 2g), B (Fig. 2k), and C (Fig. 2l) positions, and B/C (Fig. 2o). A decrease in the similarity of 2dUA spectra was observed upon titration by Gdn.HCl (Fig. 2h,i).

Sigmoid Antigen A unfolding curves and associated D_m values were obtained for A_{290}/A_{280} (2.24 ± 0.05 M), λ_{min} (2.49 ± 0.19 M), r (2.45 ± 0.06 M), RMS (2.35 ± 0.06 M) and A position (2.23 ± 0.06 M). Regarding Antigen B, sigmoid profiles were obtained for r (0.74 ± 0.02 M), RMS (0.67 ± 0.03 M), A/B (0.63 ± 0.03 M) and A/C (0.61 ± 0.03 M).

Among features associated with a sigmoid unfolding profile, priority was given to those that can be obtained from a limited data recording. In this regard, A_{290}/A_{280} was selected as the setting for monitoring unfolding for Antigen A since it does not require a whole scan to be recorded and can be calculated from absorption values obtained at two wavelengths. A/B was selected as the setting for monitoring unfolding for Antigen B since it can be obtained from a narrow scan window of 30 nm width.

Tryptophan Fluorescence Spectroscopy

TF was evaluated as a benchmark method to (2d)UA. TF has been reported to be a suitable technique for measuring protein conformational stability in a microplate (Aucamp et al., 2005), and for identify stabilizing excipients (Dasnoy et al., 2011) and ligands (Mahendrarajah et al., 2011).

With TF, a diminution of quantum yield and a red-shift in the wavelength at maximum emission have been reported to occur upon protein unfolding in an aqueous solvent. A fluorescence spectrum results from the contribution of several populations of Trp residues: the higher the exposure of a Trp residue to aqueous solvent, the higher its wavelength of emission (Lakowicz, 2004). The effect of Gdn.HCl on Trp fluorescence emission spectra was analyzed (Fig. 3a,b). The global contribution of Trp residues was assessed by monitoring F_{340} (Fig. 3c; Aucamp et al., 2005), $\langle\lambda\rangle$ (Fig. 3f), and λ_{max} (Fig. 3g) upon denaturant titration. A decrease in intensity and a red-shift were observed in the emission spectra of both antigens. Without any numerical smoothing, $\langle\lambda\rangle$ revealed to be a suitable method for monitoring changes in the shape of a spectrum (Dasnoy et al., 2011).

The relative contribution of buried and exposed Trp residue populations was assessed by difference ($F_{330} - F_{350}$; Fig. 3d) and ratio (F_{330}/F_{350}; Fig. 3e) and revealed an increase in the global exposure of Trp residues in the denatured state. Better unfolding profiles were not observed by monitoring F_{330} and F_{350} than by monitoring F_{340} (Fig. 3c).

For Antigen A, sigmoid profiles and associated D_m were obtained for F_{340} (2.15 ± 0.02 M), $F_{330} - F_{350}$ (2.18 ± 0.02 M), and $\langle\lambda\rangle$ (2.24 ± 0.03 M). F_{340} was the only feature showing a sigmoid profile upon unfolding of Antigen B (0.64 ± 0.01 M). Since F_{340} identified sigmoid unfolding profiles for both antigens, F_{340} was selected as the setting for monitoring unfolding. Hence, we confirmed the suitability of monitoring F_{340} as a fast, simple, generic, and reliable fluorescence method for measuring protein stability in microtiter plates (Aucamp et al., 2005).

High-Throughput Screening of Excipients

A HTS approach was followed to evaluate (2d)UA in the assessment of 44 excipients on protein conformational stability. Chemical unfolding (Gdn.HCl) was monitored by UA (A_{290}/A_{280}) for Antigen A and 2dUA (A/B) for Antigen B, and by TF (F_{340}) for both antigens. Thermal unfolding was monitored by DSF for Antigens A (with SO) and B (with ANS). Typical unfolding curves are illustrated in Figure 4.

A median polish procedure was applied to correct for row, column, and plate effects (Tukey, 1977). As illustrated in Figure 5 for Antigen B, this procedure corrected for the plate effect observed with 2dUA and TF, and the row effect observed with TF.

The effect of an excipient on the unfolding probe signal was analyzed by regression (Fig. 6). Basically, four different types of concentration-response to an excipient were

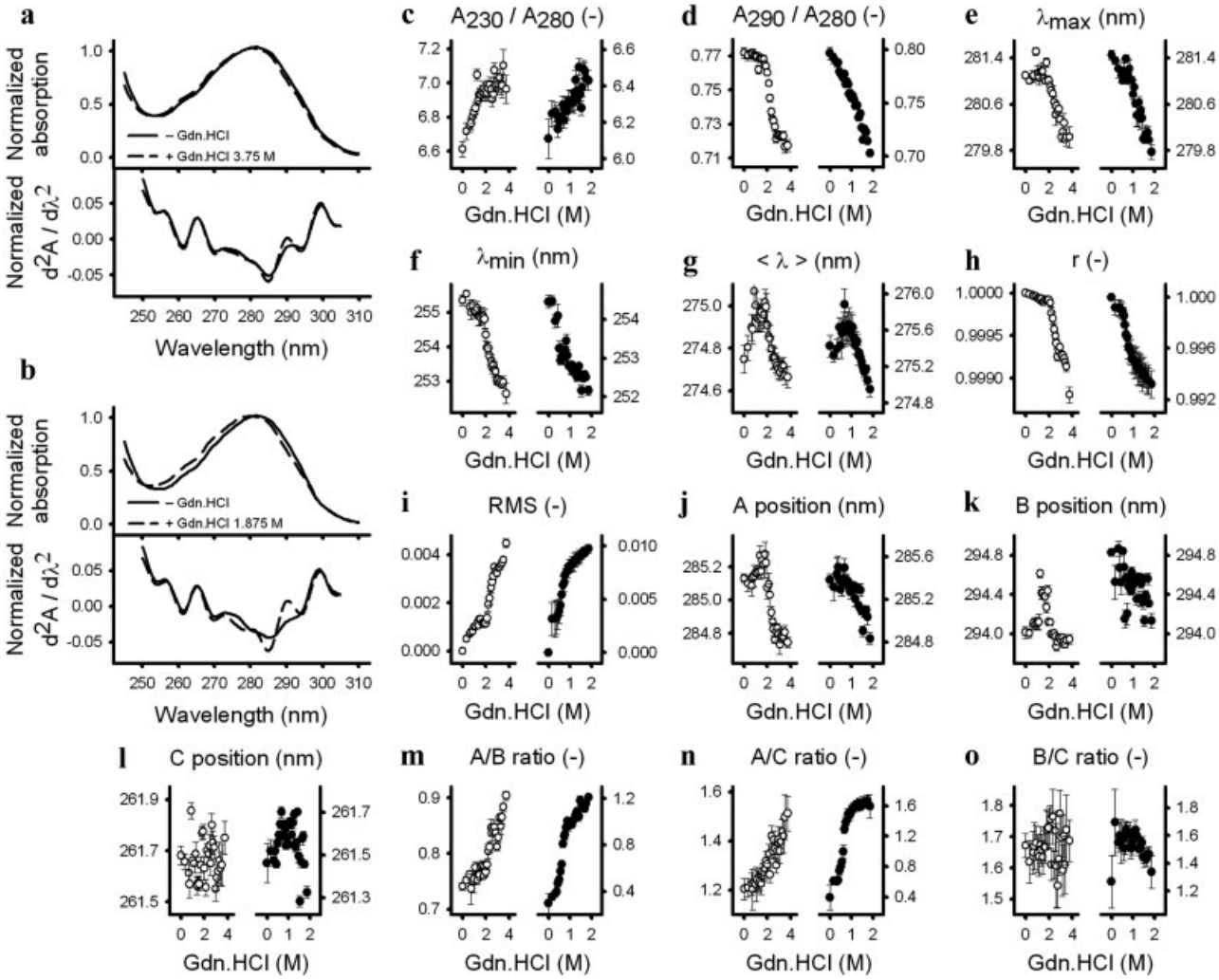

Figure 2. Unfolding probes obtained from (2d)UA spectra. Antigen A (○) and Antigen B (●) were subjected to chemical unfolding by Gdn.HCl. UA and 2dUA spectra were obtained for (**a**) Antigen A and (**b**) Antigen B. The following values were extracted from UA spectra: absorption values at (**c**) 230 and (**d**) 290 nm normalized for absorption at 280 nm, (**e**) wavelength at the maximum of absorption in the 260–290 nm range, (**f**) wavelength at the minimum of absorption in the 250–270 nm range, (**g**) center of gravity of absorption. The following values were extracted from 2dUA spectra: spectral similarity by the (**h**) correlation coefficient and (**i**) root mean square of differences methods, (**j**) Tyr/Trp peak (*A*) position in the 285 nm region, (**k**) Trp peak (*B*) position in the 295 nm region, (**l**) Phe peak (*C*) position in the 260 nm region, peak-to-valley intensity ratios of (**m**) *A/B*, (**n**) *A/C*, and (**o**) *B/C*. Error bars represent the standard deviation from eight replicate wells.

observed: nonlinear or linear, and enhanced or diminished. The six excipient-free controls present on each plate gave an indication of inter-plate variability. The median polish correction narrowed the dispersion of the controls and allowed the fitting of stronger regression models, as illustrated by better correlations between observed and predicted values. The maximal (highest or lowest depending on the excipient) predicted concentration-response was determined by regression analysis, with its associated confidence interval at 95% (Fig. 7). The excipient was considered to have a significant effect on antigen stability when the confidence interval did not span zero.

A comparison of the three analytical methods is given in Table I. The number of stabilizing excipients identified by TF and DSF, was higher than by (2d)UA. Most of stabilizing excipients were inorganic salts, sugars/polyols, or amino acids. The ranking of sugars/polyols according to their effects on antigen stability was quite similar for all three methods. For both TF and DSF analyses, the same Antigen B stabilizers were ranked in the top three.

Although $CaCl_2$ strongly stabilized Antigen B, it destabilized Antigen A. Sugars/polyols stabilized both antigens. Inositol was the superior stabilizing polyol and was ranked in the top three for all analytical methods. HP-β-CD appeared to have a destabilizing effect on both antigens. Gly, GlyGly, Lys, Ser, and Thr were observed to stabilize Antigen A using at least two analytical methods. Ala and Val were observed to slightly increase Antigen B stability using all analytical methods. His and Glu were observed to stabilize Antigen B using TF, but to destabilize it using DSF.

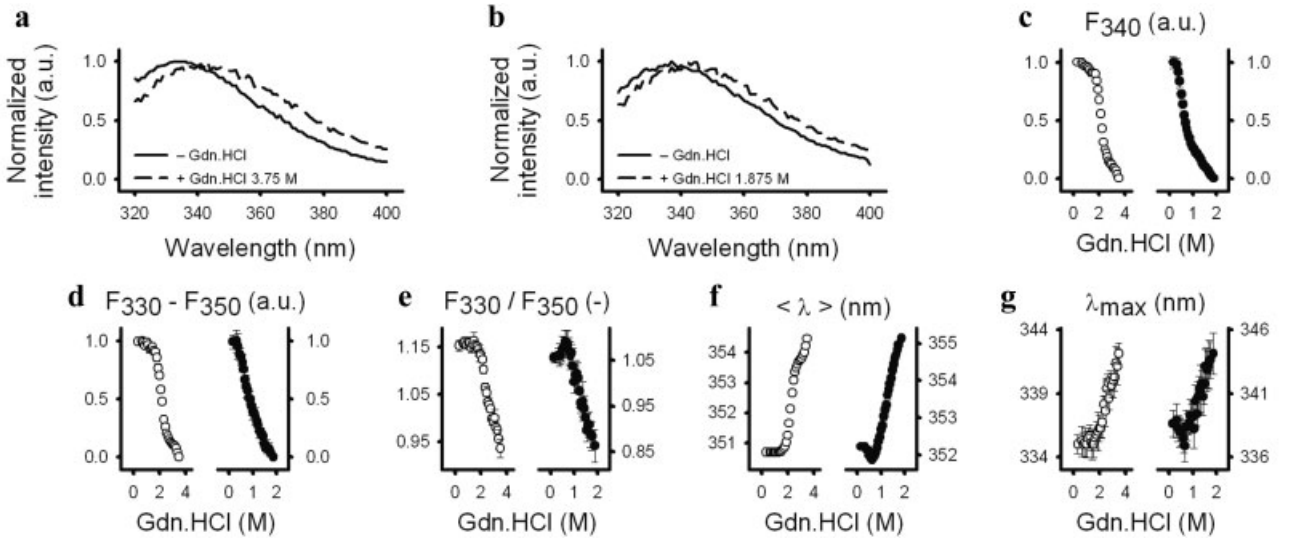

Figure 3. Unfolding probes obtained from TF emission spectra. Antigen A (○) and Antigen B (●) were subjected to chemical unfolding by Gdn.HCl. Spectra obtained for (**a**) Antigen A and (**b**) Antigen B are shown. The following values were extracted: (**c**) intensity at 340 nm, (**d**) 330–350 nm intensity difference, (**e**) 330/350 nm intensity ratio, (**f**) center of gravity of emission, and (**g**) wavelength at the maximum of emission. Error bars represent the standard deviation from eight replicate wells.

For both antigens, it was not feasible to monitor protein unfolding using DSF with high concentrations of several cyclodextrins, surfactants, and polymers. Nevertheless, surfactants and polymers had no marked effect on antigen stability using the other analytical methods. SBE-β-CD and PEGs were observed to slightly stabilize Antigen A using UA or TF. High Mw PEGs, PVPs, and Myrj52 were observed to destabilize Antigen B using 2dUA and TF.

For Arg concentrations $\geq$50 mM with Antigen A, a sigmoid transition was not observed; whereas a sigmoid transition was not observed for all Arg concentrations with Antigen B, irrespective of the analytical method. This different antigen-dependent response to excipient concentration was also observed with sodium docusate, where a sigmoid transition was not observed with sodium docusate concentrations $\geq$0.008% for Antigen A and was not observed with all sodium docusate concentrations for Antigen B.

Validation of HTS Assays for Antigen B

The highest predicted effect on Antigen B conformational stabilization was obtained with 50 mM $CaCl_2$ by all analytical methods. To estimate the width of the screening window, a post-screening *z*'-factor was calculated (Zhang et al., 1999) by filling a single microplate with randomly distributed controls (Dasnoy et al., 2011). Positive and negative controls were 50 mM $CaCl_2$ (highest predicted effect) and buffer alone (no effect), respectively. Results are shown in Figure 8. The *z*'-factors calculated for all assays were greater than 0.5, indicating that all analytical methods were valid for identifying stabilizing excipients (Zhang et al., 1999). The median polish correction applied to each control was found to lower variability and therefore increase *z*'-factors.

Confirmation of Stabilizing Excipients

The excipients predicted to significantly stabilize an antigen according to at least 2 out of the 3 analytical methods were selected for further characterization. The effect of these excipients on the conformational stability of both antigens was evaluated by isothermal stability at 45°C (Fig. 9). A set of extrinsic fluorescent dyes were evaluated for their ability to detect conformational changes (data not shown). The unfolding of Antigens A and B was monitored by SO and bis-ANS, respectively. Sample aggregation state was assessed by OD_{350}. Although an increase in Antigen A unfolding was observed after 30 min (Fig. 9a), no increase in Antigen A aggregation was observed, even after overnight incubation at 45°C (data not shown). For Antigen B, the increase in unfolding over time preceded the increase in aggregation over time (Fig. 9b). Therefore, bis-ANS emission appeared to be a more sensitive method than OD_{350} for studying the effect of hydrophilic excipients on Antigen B isothermal stability.

All of the studied excipients limited protein unfolding. Moreover, Lys with Antigen A and $CaCl_2$ and Pro with Antigen B did not increase protein affinity for the fluorescent dye (extrinsic unfolding probe). All polyols stabilized Antigen B but had minimal stabilizing effects on Antigen A. Polyols stabilized Antigen B better than trehalose. The stabilizing effect conferred by the amino acid excipients were ranked as follow: Lys > GlyGly > Ser = Thr > Gly (for Antigen A) and Pro > Ala > Val > Gly (for Antigen B).

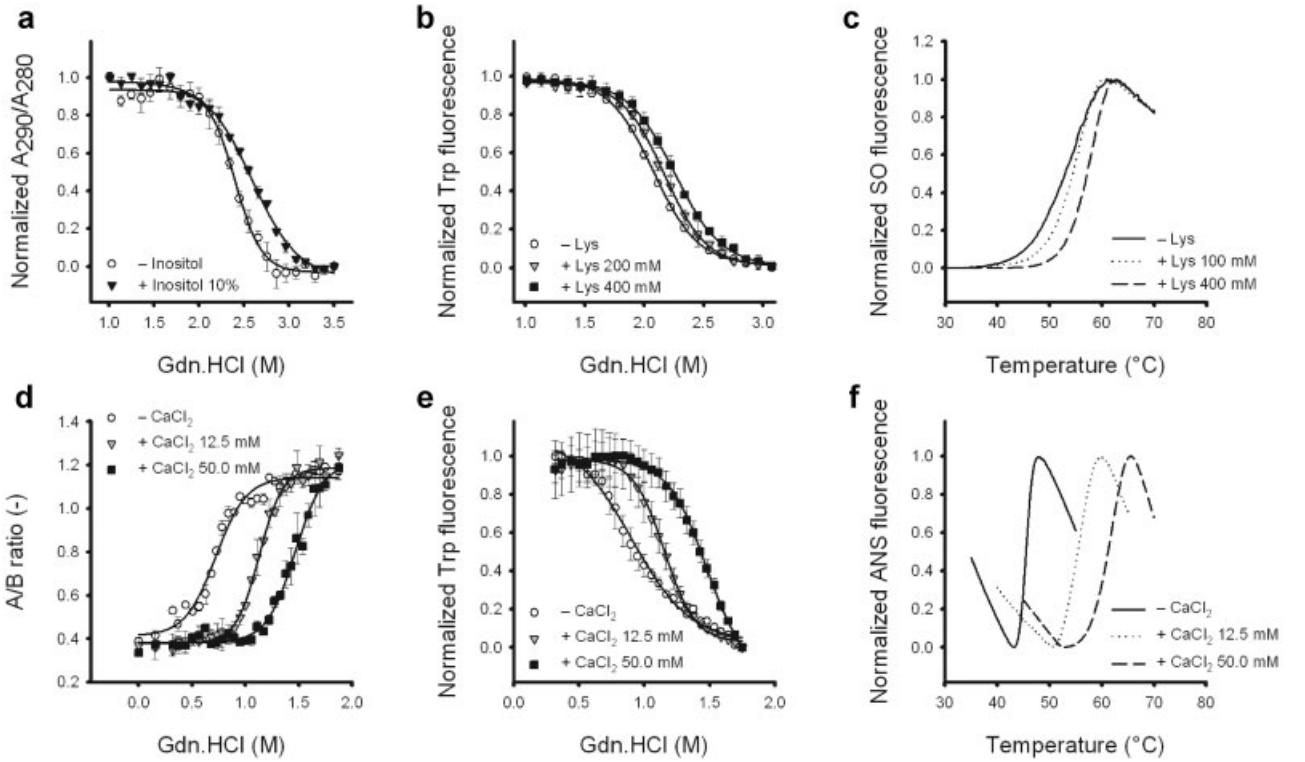

Figure 4. Effect of excipients on the denaturation profiles of Antigens A and B. Antigen A denaturation monitored by (**a**) 290 to 280 nm absorption ratio from UA, (**b**) Trp emission intensity at 340 nm, and (**c**) SO intensity from DSF are shown. Antigen B denaturation monitored by (**d**) *A*/*B* peak-to-valley intensity ratio from 2dUA (**e**) Trp emission intensity at 340 nm, and (**f**) ANS intensity from DSF are shown. Data were fitted to a Boltzmann sigmoid function. Error bars represent the standard deviation from three wells located on different plates.

Discussion

The conformational stabilities of two antigenic proteins were evaluated in microplates by two label-free spectroscopic techniques, TF and (2d)UA. Trp was used as an intrinsic probe for monitoring the unfolding of both antigens by fluorescence spectroscopy (Fig. 3c) and allowed the identification of stabilizing excipients. Hence, monitoring F_{340} was confirmed as a suitable setting for assessing protein conformational stability in microplates (Aucamp et al., 2005). Trp absorption, monitored by the decrease of A_{290}/A_{280}, was used to measure Antigen A unfolding (Fig. 2d; Lakowicz, 2004).

Although selective excitation of Tyr remains a challenge for fluorescence spectroscopy of Trp-containing proteins (Lakowicz, 2004), Tyr absorption spectroscopy using 2dUA (because Tyr absorption is altered by its exposure to an aqueous environment; Ragone et al., 1984) was shown to be a suitable probe for monitoring Antigen B unfolding (Fig. 2m). In contrast to TF, 2dUA offers the possibility to monitor each aromatic amino acid residue individually as an unfolding probe. Moreover, based on spectral similarity measurements (Park et al., 1989; Prestrelski et al., 1993), we propose a method to monitor simultaneously the global changes occurring in the Phe, Tyr, and Trp amino acid residue environments by comparisons of 2dUA spectra from samples subjected or not subjected to stress conditions (Fig. 2h,i).

The high sensitivity of fluorescence-based methods make them attractive for studying protein antigens at low concentrations and typical of antigen concentrations found in vaccines (Dasnoy et al., 2011). TF is a label-free method by which a global assessment is made of all Trp residues present in the sample, from both folded and unfolded protein molecules. Hence, TF may not be sufficiently sensitive to detect denaturation if only a small proportion of the protein molecules are unfolded. In contrast, DSF should only detect unfolded protein molecules and should therefore be more sensitive than TF. However, this sensitivity may be compromised by the hydrophobic dye used in DSF; because the dye may perturb the conformation of protein molecules. The interaction between the dye and certain cyclodextrins, polymers, and surfactants also impaired DSF measurements (Fig. 7). For the analysis of Antigen B using DSF, silicon oil was added to prevent evaporation in 384-well microplates and may have affected protein conformation at the oil/sample interface. Nevertheless, in terms of rapidity and ease of

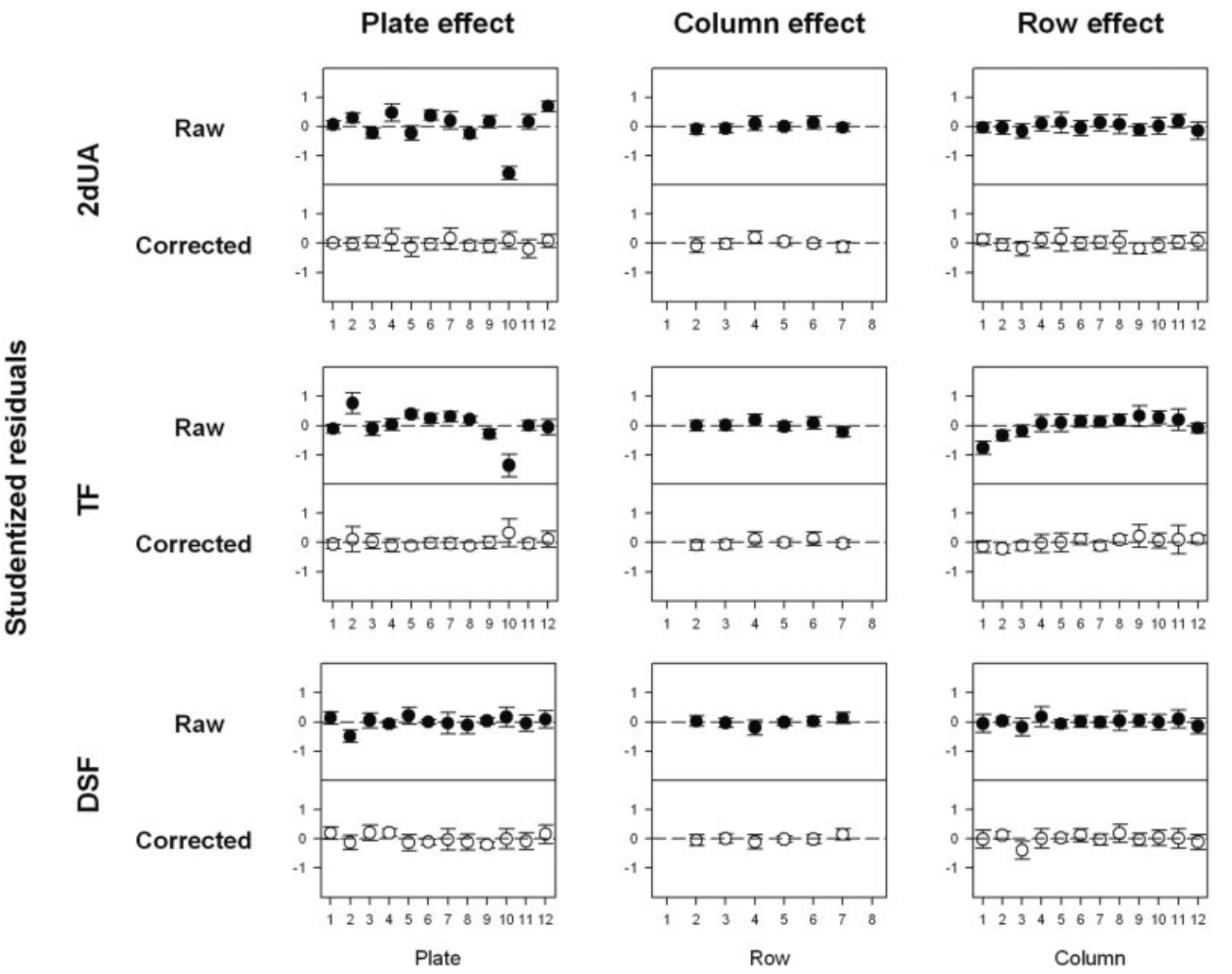

Figure 5. Effect of the median polish correction on the plate, row, and column effects obtained in the Antigen B screening by 2dUA, TF, and DSF. Graph of studentized residuals: standardized residual information obtained after removal of predicted excipients effects, with raw (●) and corrected (○) values. Error bars represent the least-square differences.

use with small hydrophilic excipients, DSF was confirmed as an efficient analytical method (Senisterra and Finerty, 2009).

Improved resolution (Fig. 8) and better regression models (Fig. 6) were obtained by applying the median polish correction in HTS studies. The randomized positional allocation of samples in the microplates meant that distorting plate, row, and column effects were suppressed. For example, the lower D_m values obtained with Plate 10 by UA and TF (Fig. 5) could have been due to a dilution error when preparing the Gdn.HCl stock solution. If raw data from Plate 10 had been used, these data would have been probably discarded from the screening data. Therefore, randomized sample allocation and the median polish correction should increase the probability of identifying stabilizing excipients.

Stabilizing excipients were mainly identified among salts, sugars, and amino acids. These families of compounds are known to protect proteins by preferential exclusion (Arakawa and Timasheff, 1985). In contrast, HP-β-CD was a destabilizing excipient with both antigens, perhaps through its preferential stabilization of unfolded proteins (Tavornvipas et al., 2006).

The absence of unfolding sigmoid transitions when using Arg or sodium docusate suggests that these excipients alter the conformation of the two antigens. Arg has been reported to preferentially interact with most amino acid residues and peptide bonds (Arakawa et al., 2007). Ionic surfactants, such as sodium docusate, are known to denature proteins even at low concentration (Sellers and Maa, 2005).

His and Glu had opposite effects on Antigen A depending on whether the antigen was chemically (stabilization) or

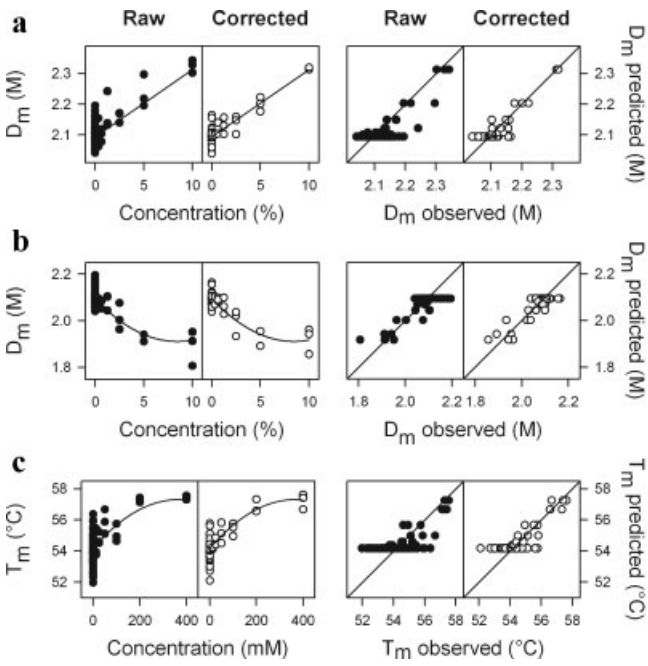

Figure 6. Data analysis strategy for studying the effect of excipient concentration on D_m and T_m: example of the effect of (**a**) inositol, (**b**) HP-β-CD and (**c**) Lys on Antigen A stability. Raw data before (●) and after (○) correction with the median polish procedure were analyzed by regression. The regression model was built from corrected data and allowed the prediction of D_m or T_m for a given excipient concentration. The quality of the prediction model was assessed by measuring Q^2 as an indicator of the correlation between observed and predicted D_m or T_m values.

thermally induced (destabilization) to unfold. Hence, protein antigens may behave in different way upon chemical and thermal unfolding. No aggregation was detected by OD_{350} during chemical unfolding, but there may have been a higher propensity to aggregate during thermal unfolding reflected by a T_m decrease and a potential manifestation of the shift from native to aggregated species. This T_m decrease may be due to the presence of excipient but also to a pH change, since the presence of His or Glu at their maximal concentration (400 mM) decreased the pH from 6.83 ± 0.06 to 5.70 ± 0.02 and 3.75 ± 0.07, respectively ($n = 3$).

An objective way of comparing analytical methods used in HTS is through the calculation of their respective *z*'-factors. This was performed by analysing the stabilizing effect of $CaCl_2$ on Antigen B (Fig. 8). Despite the higher sensitivity of fluorescence-based methods, all techniques had a comparable screening window. The median polish correction improved the resolution of all screening assays.

The fluorescent dye operates as extrinsic probe to allow monitoring protein unfolding in the isothermal stability assay (Senisterra et al., 2008) and monitoring protein unfolding was more sensitive than monitoring protein aggregation by OD_{350} (Fig. 9). An increase in Antigen B surface hydrophobicity (bis-ANS emission) preceded Antigen B aggregation (OD_{350}; Fig. 9b), and confirms that a conformational change is required for aggregation (Dasnoy et al., 2011; Wang, 2005). The more stabilizing excipients found in isothermal stability studies were Lys for Antigen A, and both $CaCl_2$ and Pro for Antigen B (Fig. 9). All of the analytical methods used during excipient screening predicted the stabilizing effect of these compounds (Fig. 7). Among the three best compounds predicted by HTS studies (Table I), $CaCl_2$ was identified as the best Antigen B stabilizer by all the analytical methods, whereas only DSF ranked Pro for Antigen B, and Lys for Antigen A in the top three. Since both thermal (used in combination with DSF) and isothermal unfolding methods are based on the principle of heating a sample in the presence of a hydrophobic dye, it may not be surprising that the same compounds were ranked high by both approaches. The performance of excipients identified by extrinsic fluorescence techniques should be confirmed by label-free methods. Although inositol was ranked among the three best-stabilizing excipients for both antigens by all analytical methods (Table I), this compound offered limited protein protection in isothermal stability studies (Fig. 9).

Unfortunately, no general rule exists to predict the best-stabilizing excipient for a given protein. The choice of excipients is generally performed on an empirical basis. Measuring protein conformational stability by chemical or thermal unfolding is a powerful approach for the identification of stabilizing excipients. Based on the screening results obtained by (2d)UA, TF, and DSF, as well as on isothermal stability studies, Lys and $CaCl_2$ were found to be the best excipients for stabilizing Antigens A and B, respectively. These protein-specific excipients would probably not have been prioritised for evaluation by classical formulation approaches. Our results highlight the usefulness of HTS methods for rapidly evaluating a broad choice of excipients in samples containing low protein concentrations.

Conclusions

This study demonstrates that both UA spectra recorded in microplate and their calculated 2dUA spectra provide various features that can be used as protein stability indicators. Relevant (2d)UA spectral features were selected for two antigens and evaluated in their ability to identify stabilizing excipients upon chemically induced unfolding. (2d)UA was compared with analytical methods commonly used in protein stability studies: a chemically induced unfolding and screening-based method similar to (2d)UA but monitored by TF, and a thermally induced unfolding method monitored by DSF. The random positional distribution of samples in microplates allowed the use of a median polish procedure to correct for plate, row, and column effects. Applying these corrections improved the quality of prediction models and the screening resolution. Irrespective of the unfolding method applied, similar

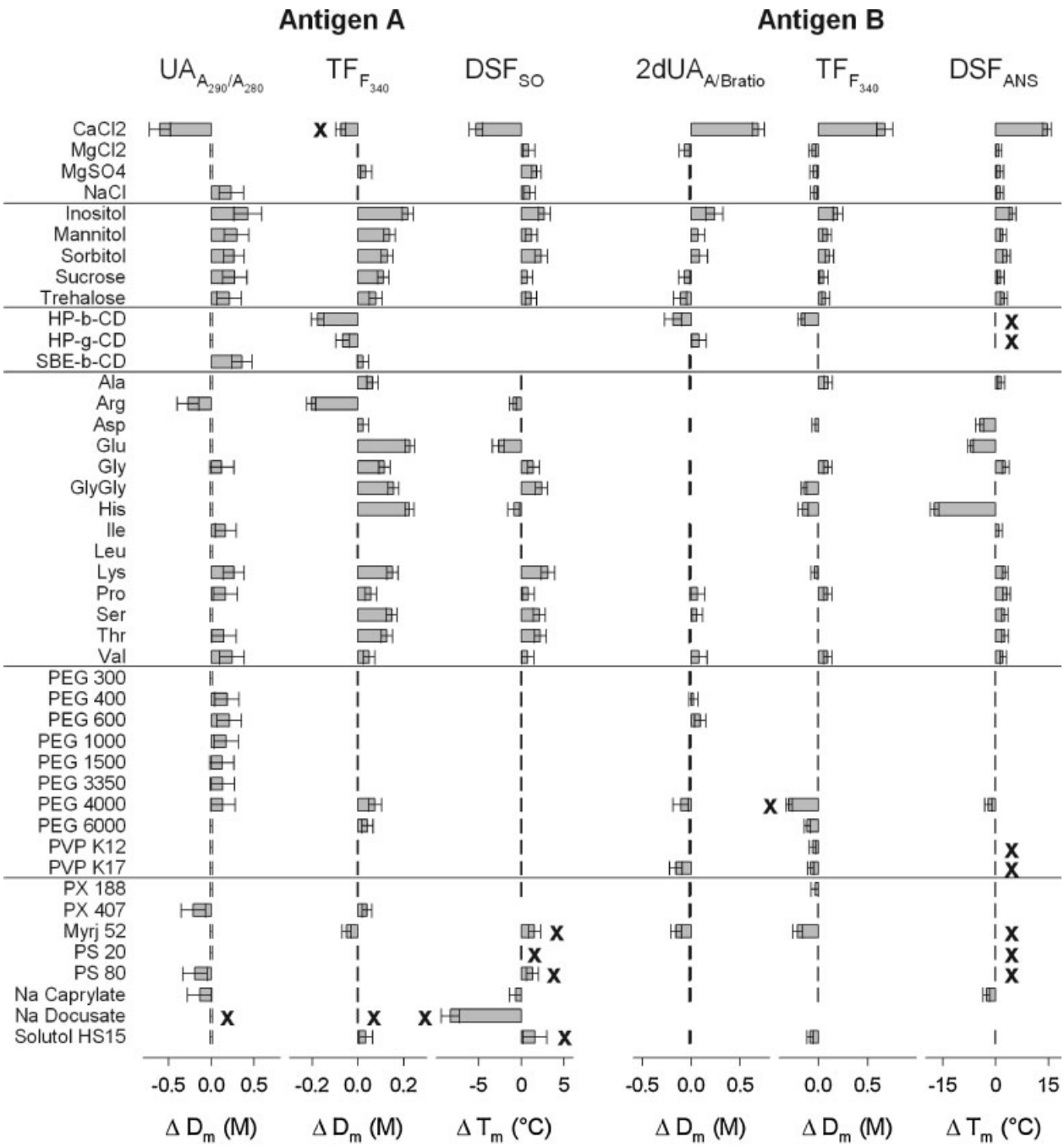

Figure 7. High-throughput screening of excipients for stabilizing Antigens A and B. D_m was calculated from 290 to 280 nm absorption ratio from UA spectra (Antigen A) or by *A/B* peak-to-valley intensity ratio from 2dUA spectra (Antigen B), and by emission intensity at 340 nm in TF. T_m was measured by SO (Antigen A) or ANS (Antigen B) emission intensity in DSF. Horizontal bars represent the highest or lowest value predicted by regression analysis and its confidence interval at 95%. An absence of prediction indicates that no sigmoid unfolding pattern was observed or no significant effect was predicted at any excipient concentration. A *X* symbol indicates that the high concentrations of excipients were discarded from the regression analysis, because of missing values which may lead to inappropriate extrapolations.

Table I. Comparison of HTS results obtained by (2d)UA, TF, and DSF.

Antigen	Stabilizing excipients	(2d)UA	TF	DSF
A	Number	15	20	17
	3 Superior	Inositol > SBE-β-CD > Mannitol	Glu > His > Inositol	Lys > Inositol >GlyGly
B	Number	7	10	16
	3 Superior	$CaCl_2$ > Inositol > PEG600	$CaCl_2$ > Inositol > Sorbitol	$CaCl_2$ > Inositol > Sorbitol = Pro

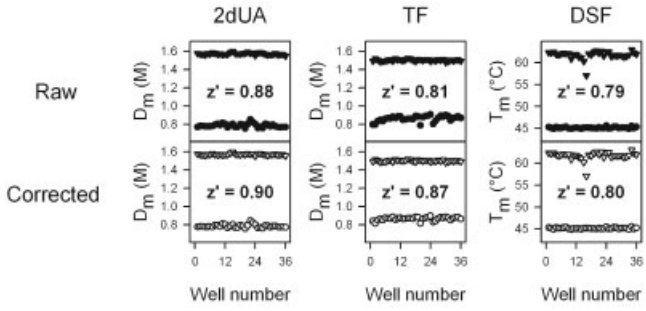

Figure 8. Validation of HTS assays used for Antigen B by calculation of associated *z'*-factors. The controls were buffer (●) and $CaCl_2$ 50 mM (▲). Buffer (○) and $CaCl_2$ 50 mM (△) values obtained after a median polish correction are shown. Values were obtained from a single microplate.

stabilizing excipients were identified by all analytical methods. A higher sensitivity of TF and DSF, both fluorescence-based methods, allowed the identification of a larger number of stabilizing excipients than (2d)UA. DSF could not be used to study hydrophobic excipients due to hydrophobic excipient interactions with dye molecules. A

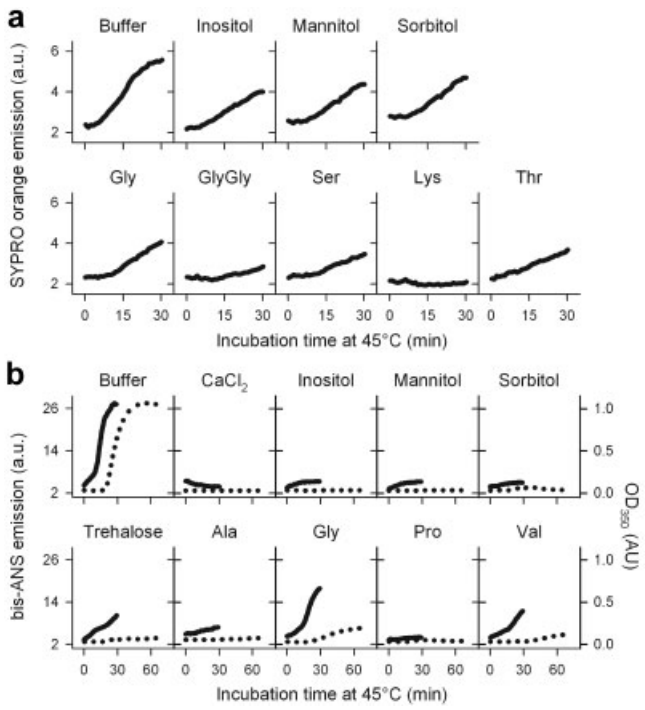

Figure 9. Effect of selected excipients on the stability of Antigens A and B at 45°C. Averages curves obtained from three independent experiments are shown. **a**: Antigen A was monitored by SO fluorescence emission. The relative standard deviation of the assay calculated from three independent experiments (RSD) was 3.95 ± 0.67%. **b**: Antigen B was monitored by bis-ANS fluorescence emission (RSD = 7.94 ± 2.77%, solid line) and optical density at 350 nm (RSD = 7.07 ± 3.99%, dotted line). The concentrations were the following: 10% sugar and polyols, 400 mM amino acids, 50 mM $CaCl_2$.

HTS of excipients tested with Antigen B showed a similar screening resolution (*z'*-factor > 0.8) with the three analytical methods; 2dUA, TF, and DSF. Therefore, (2d)UA deserves more attention in HTS studies focused on protein conformational stability.

This work was supported by GlaxoSmithKline Biologicals. The authors thank BASF, CyDex, Roquette, and Sasol for providing gift samples of excipients. Ulrike Krause, Pascal Cadot, and Matthew Morgan are acknowledged for their support in reviewing the article.

References

Arakawa T, Timasheff SN. 1985. The stabilization of proteins by osmolytes. Biophys J 47:411–414.

Arakawa T, Ejima D, Tsumoto K, Obeyama N, Tanaka Y, Kita Y, Timasheff SN. 2007. Suppression of protein interactions by arginine: A proposed mechanism of the arginine effects. Biophys Chem 127:1–8.

Aucamp JP, Cosme AM, Lye GJ, Dalby PA. 2005. High-throughput measurement of protein stability in microtiter plates. Biotechnol Bioeng 89:599–607.

Ausar SF, Espina M, Brock J, Thyagarayapuran N, Repetto R, Khandke L, Middaugh CR. 2007. High-throughput screening of stabilizers for respiratory syncytial virus: Identification of stabilizers and their effects on the conformational thermostability of viral particles. Hum Vaccin 3:94–103.

Capelle MA, Gurny R, Arvinte T. 2009. A high throughput protein formulation platform: Case study of salmon calcitonin. Pharm Res 26:118–128.

Dasnoy S, Dezutter N, Lemoine D, Le Bras V, Préat V. 2011. High-throughput screening of excipients intended to prevent antigen aggregation at air–liquid interface. Pharm Res 28:1591–1605.

Eftink MR. 2000. Use of fluorescence spectroscopy as thermodynamics tool. Methods Enzymol 323:459–473.

He F, Joshi SB, Moore DS, Shinogle HE, Ohtake S, Lechuga-Ballesteros D, Martin RA, Truong-Le VL, Middaugh CR. 2010. Using spectroscopic and microscopic methods to probe the structural stability of human adenovirus type 4. Hum Vaccin 6:202–211.

Hermeling S, Crommelin DJ, Schellekens H, Jiskoot W. 2004. Structure–immunogenicity relationships of therapeutic proteins. Pharm Res 21:897–903.

Kissmann J, Ausar SF, Foubert TR, Brock J, Switzer MH, Detzi EJ, Vedvick TS, Middaugh CR. 2008a. Physical stabilization of Norwalk virus-like particles. J Pharm Sci 97:4208–4218.

Kissmann J, Ausar SF, Rudolph A, Braun C, Cape SP, Sievers RE, Federspiel MJ, Joshi SB, Middaugh CR. 2008b. Stabilization of measles virus for vaccine formulation. Hum Vaccin 4:350–359.

Kueltzo LA, Normand N, O'Hare P, Middaugh CR. 2000. Conformational lability of herpesvirus protein VP22. J Biol Chem 275:33213–33221.

Lakowicz JR. 2004. Principles of fluorescence spectroscopy. New York: Springer. 725 p.

Leach SJ, Scheraga HA. 1960. Effect of light scattering on ultraviolet difference spectra. J Am Chem Soc 82:4790–4792.

Liu PF, Avramova LV, Park C. 2009. Revisiting absorbance at 230nm as a protein unfolding probe. Anal Biochem 389:165–170.

Mach H, Middaugh CR. 2011. Ultraviolet spectroscopy as a tool in therapeutic protein development. J Pharm Sci 100:1214–1227.

Mahendrarajah K, Dalby PA, Wilkinson B, Jackson SE, Main ERG. 2011. A high-throughput fluorescence chemical denaturation assay as a general screen for protein-ligand binding. Anal Biochem 411:155–157.

Malo N, Hanley JA, Carlile G, Liu J, Pelletier J, Thomas D, Nadon R. 2010. Experimental design and statistical methods for improved hit detection in high-throughput screening. J Biomol Screen 15:990–1000.

McGown EL, Hafeman DG. 1998. Multichannel pipettor performance verified by measuring pathlength of reagent dispensed into a microplate. Anal Biochem 258:155–157.

Pace CN, Scholtz JM. 1997. Measuring the conformational stability of a protein. In: Creighton TE, editor. Protein structure: A practical approach. New York: Oxford University Press. p 299–321.
Park MK, Park JH, Cho JH. 1989. Qualitative analysis by derivative spectrophotometry (II). Computer-assisted spectral analysis using derivative spectra and root mean of squares of differences. Arch Pharm Res 12:289–294.
Peek LJ, Brey RN, Middaugh CR. 2007. A rapid, three-step process for the preformulation of a recombinant ricin toxin A-chain vaccine. J Pharm Sci 96:44–60.
Prestrelski SJ, Arakawa T, Carpenter JF. 1993. Separation of freezing- and drying-induced denaturation of lyophilized proteins using stress-specific stabilization. II. Structural studies using infrared spectroscopy. Arch Biochem Biophys 303:465–473.
Ragone R, Colonna G, Balestrieri C, Servillo L, Irace G. 1984. Determination of tyrosine exposure in proteins by second-derivative spectroscopy. Biochemistry 23:1871–1875.
Savitzky A, Golay MJE. 1964. Smoothing and differentiation of data by simplified least squares procedures. Anal Chem 36:1627–1639.
Sellers SP, Maa YF. 2005. Principles of biopharmaceutical protein formulation: an overview. Methods Mol Biol 308:243–263.
Senisterra GA, Finerty PJ. 2009. High throughput methods of assessing protein stability and aggregation. Mol Biosyst 5:217–223.
Senisterra GA, Soo HB, Park HW, Vedadi M. 2008. Application of high-throughput isothermal denaturation to assess protein stability and screen for ligands. J Biomol Screen 13:337–342.
Shire SJ. 2009. Formulation and manufacturability of biologics. Curr Opin Biotechnol 20:708–714.
Tavornvipas S, Hirayama F, Takeda S, Arima H, Uekama K. 2006. Effects of cyclodextrins on chemically and thermally induced unfolding and aggregation of lysozyme and basic fibroblast growth factor. J Pharm Sci 95:2722–2729.
Thirumangalathu R, Krishnan S, Bondarenko P, Speed-Ricci M, Randolph TW, Carpenter JF, Brems DN. 2007. Oxidation of methionine residues in recombinant human interleukin-1 receptor antagonist: Implications of conformational stability on protein oxidation kinetics. Biochemistry 46:6213–6224.
Thirumangalathu R, Krishnan S, Ricci MS, Brems DN, Randolph TW, Carpenter JF. 2009. Silicone oil- and agitation-induced aggregation of a monoclonal antibody in aqueous solution. J Pharm Sci 98:3167–3181.
Thomson JA, Shirley BA, Grimsley GR, Pace CN. 1989. Conformational stability and mechanism of folding of ribonuclease T1. J Biol Chem 264:11614–11620.
Tukey JW. 1977. Exploratory data analysis. Reading: Addison-Wesley. 688 p.
Vessely C, Estey T, Randolph TW, Henderson I, Cooper J, Nayar R, Braun LJ, Carpenter JF. 2009. Stability of a trivalent recombinant protein vaccine formulation against botulinum neurotoxin during storage in aqueous solution. J Pharm Sci 98:2970–2993.
Wang W. 2005. Protein aggregation and its inhibition in biopharmaceutics. Int J Pharm 289:1–30.
Zhang JH, Chung TD, Oldenburg KR. 1999. A simple statistical parameter for use in evaluation and validation of high throughput screening assays. J Biomol Screen 4:67–73.
Zhao H, Graf O, Milovic N, Luan X, Bluemel M, Smolny M, Forrer K. 2010. Formulation development of antibodies using robotic system and High-Throughput Laboratory (HTL). J Pharm Sci 99:2279–2294.